Structural Properties of VOTTDPZ Investigated by means of STM

Master Thesis

Simon Emil Nielsen

Aalborg University
Department of Materials and Production

Department of Materials and Production
Aalborg University
https://www.mp.aau.dk/

AALBORG UNIVERSITY
STUDENT REPORT

Title:
Structural Properties of VOTTDPz Investigated by means of STM

Theme:
Scientific Theme

Project Period:
Fall Semester 2019 and Spring Semester 2020

Project Group:
5.336

Participant(s):
Simon Emil Nielsen

Supervisor(s):
Lars Diekhöner

Copies: 1

Page Numbers: 50

Date of Completion:
December 13, 2020

Abstract:

By means of Scanning Tunneling Microscopy the structural properties of vanadyl tetrakis(thiadiazole) porphyrazine (VOTTDPz), which is a derivate molecule of the well-studied Phthalocyanine-family, is investigated. The molecules are deposited and subsequently investigated on the noble metal-surfaces; Ag(111) and Au(111). How the degree of molecule-coverage affects the structural and electronic properties is here investigated on the two substrates and compared. Controlling the structural electronic as well as magnetic properties of this type of metal-organic adsorbate is paramount for realizing smaller electronic and spin-tronic devices. Furthermore the chemical and magnetic properties of VOTTDPz are investigated at the University of Copenhagen in collaboration with Professor Jesper Bendix.

Contents

Preface **vii**

1 Introduction **1**

1.1 Self-assembly and Self-organisation of Molecules on Metallic Substrates . . . 1

1.2 VOPc and VOTTDPz Investigated on Metallic Substrates . . . 4

1.2.1 Metal Phthalocyanines . . . 5

1.2.2 Metal tetrakis(thiadiazole) phorpyrazine . . . 8

1.2.3 Vanadyl tetrakis(thiadiazole) phorpyrazine . . . 8

2 Methods and Experimental Setup **13**

2.1 Experiments Performed at the University of Copenhagen . . . 13

2.1.1 Powder X-ray Diffraction . . . 13

2.1.2 Electron Paramagnetic Resonance . . . 13

2.1.3 Magnetic Measurements . . . 14

2.2 The Ultra High Vacuum System and Preparation of Samples . . . 14

2.2.1 The Ultra High Vacuum System . . . 14

2.2.2 Sample Cleaning Process . . . 15

2.3 Deposition of Molecules . . . 15

2.3.1 Preparation of Molecules before Deposition . . . 15

2.3.2 Deposition of VOTTDPz . . . 17

2.3.3 Annealing after Deposition of VOTTDPz . . . 18

2.4 The Scanning Tunneling Microscope . . . 19

2.5 Tunneling Theory . . . 20

2.5.1 1-dimensional Time Independent Model . . . 21

2.5.2 3-dimensional Tershoff-Hamann Model . . . 23

2.5.3 Scanning Tunneling Spectroscopy . . . 24

2.5.4 Surface States of the Ag(111) and Au(111) Surfaces . . . 24

3 Results and Discussion **27**
3.1 Results Obtained from Experiments Carried out at the University of Copenhagen . . . 27
3.1.1 Powder X-ray Diffraction performed on VOTTDPz . . . 27
3.1.2 Electron Paramagnetic Resonance performed on VOTTDPz in DMSO solution . . . 28
3.1.3 Magnetic Measurements . . . 29
3.2 VOTTDPz deposited on Au(111) . . . 30
3.2.1 Deposition after Degassing . . . 30
3.2.2 Investigation of Bias and Tunnel Current Dependency . . . 33
3.2.3 Annealing at Low Temperatures of VOTTDPz/Au(111) System 39
3.3 VOTTDPz deposited on Ag(111) . . . 39
3.3.1 Annealing at Low Temperatures on the VOTTDPz/Ag(111) System . . . 44

4 Conclusion, Summary and Outlook **47**

Bibliography **49**

Preface

This project was conducted over the period of the 3rd September 2019 to the 13th of December 2020, by Simon Emil Nielsen as the final thesis of the MSc in Engineering in Nanomaterials and Nanophysics at the Department of Materials and Production of Aalborg University. Supervising this project was associate professor, Lars Diekhöner, without whom this project would have been impossible to realise. I am very grateful for the patience and level of understand he has shown, and the ability to guide me through till the end. I also want to thank Professor Jesper Bendix, from the University of Copenhagen, for giving me the opportunity to investigate a very interesting molecule by means of STM as well as at the University of Copenhagen. This collaboration was very interesting and exciting. Furthermore a tribute should be paid to Peter Kjær for always filling the nitrogen-tank, keeping the STM cooled.

Citations to literature is denoted by numbers in square brackets. Here the number represents order of first appearance, which is also how they are listed in the bibliography. The citation-style is American Psychological Association 7th edition (APA). Software used in this project includes Gwyddion in the analysis of the topographies obtained, GIMP 2.0 for adapting images and creating schematics and STMAFM to control the STM and STS.

Aalborg University, December 13, 2020

Simon Emil Nielsen
seni14@student.aau.dk

Chapter 1

Introduction

This report is structured as follows: Chapter 1 is denoted to reviewing state of the art experiments carried out on Phthalocyanine as well as Vanadyl Tetrakis (Thiadiazole)Porphyrazine laying the foundation for the experiments and results presented in this study. An understanding for the molecule VOTTDPz should be achieved as well. Chapter 2 is denoted to the explanation of the experimental setup, and the methods used in this project to obtain the results presented in Chapter 3. Furthermore an understanding of the Scanning Tunneling Microscope should be obtained. Chapter 3 is denoted to the represent and discuss the experimental data gathered throughout this study. And lastly Chapter 4 is denoted to conclude on the findings of this study as well as present possible things to improve and further investigate in future works.

1.1 Self-assembly and Self-organisation of Molecules on Metallic Substrates

In order to study and tailor self-assembled and self-organised structures an understanding of the novel intermolecular interactions as well as the interactions between the molecule and substrate is needed. Firstly a definition of the terms self-assembly and self-organisation is necessary to understand some of the dynamics that are taking place on the metallic substrate. Self-assembly can be defined as: *"Molecular self-assembly is the spontaneous association of molecules under equilibrium conditions into stable, structurally well-defined aggregates joined by noncovalent bonds."*[1]. Here the self-assembled structures of the molecules are reversible, meaning weak bonds between the molecules can be formed and broken until a stable equilibrium assembly is met. Self-organisation on the other hand is described as a state, where the molecules gets "trapped" in the process of finding a global energy-minimum, resulting in a sort of *"frozen state"*[2].

A balance between molecule-molecule and molecule-substrate interactions have to be found in order for self-assembly to be realised. This balance can be expressed in terms of energy in the following way:

$$E_b > E_{inter} \geq E_{kin} > E_d \tag{1.1}$$

[2]

where E_b is the energy of the bond between molecule and substrate, E_{inter} is the intermolecular energy,E_{kin} is the kinetic energy of a molecule at the surface and E_d is the diffusion energy barrier. To form a stable self-assembled structure the energy of the diffusion energy barrier has to be overcome, which can be done by controlling the temperature of the substrate, leading to a higher kinetic energy of the molecules at the surface. With a kinetic energy of the molecules higher than the diffusion barrier energy, the molecules can now probe the energy landscape that exists on the surface, in order to find a global energy-minimum. Here it is understood that the kinetic energy of the molecules cannot exceed the molecule-surface binding energy, which would lead to the molecules desorbing from the surface. Now for the energy, E_{inter}, crucial for forming stable self-assembled entities. This energy should be relatively "weak", since E_{inter} too high would result in the molecules binding to each other irreversibly. That said the intermolecular binding energy has to be in the same order (and slightly higher) as the kinetic energy of the molecules, in order to form bonds between molecules and ultimately a self-assembled network of molecules.
If the molecules do not have sufficiently high kinetic energy to break the diffusion energy barrier, they will not be able to search the energy landscape properly resulting in a quick adsorption to the surface.

Self-assembly and self-organization can be understood visually, as seen in Figure 1.1.

On the left side a high flux of molecules is applied, but the diffusivity is low, which could be a result of a very low substrate temperature. A substrate with a low temperature will not transfer much energy to the molecules, which will result in the kinetic energy of the molecules being too low to break the diffusion energy barrier. As can be seen in the figure, the blue molecules on the left side will hit the substrate, and quickly adsorb to the substrate resulting in many small growth-sites consisting of few molecules. This situation is diffusion-limited self-organization. Here it is important to notice that the molecules exactly is in a sort of frozen state, which does not allow them to find a global energy-minimum, resulting in a system that is not in equilibrium. On the right side the flux is lower compared to the left side, but here a high diffusivity is realised. When the molecules hit the substrate, they have enough kinetic energy to diffuse on the surface of the substrate in search of the most energetically favorable situation. This results in fewer growth-sites,

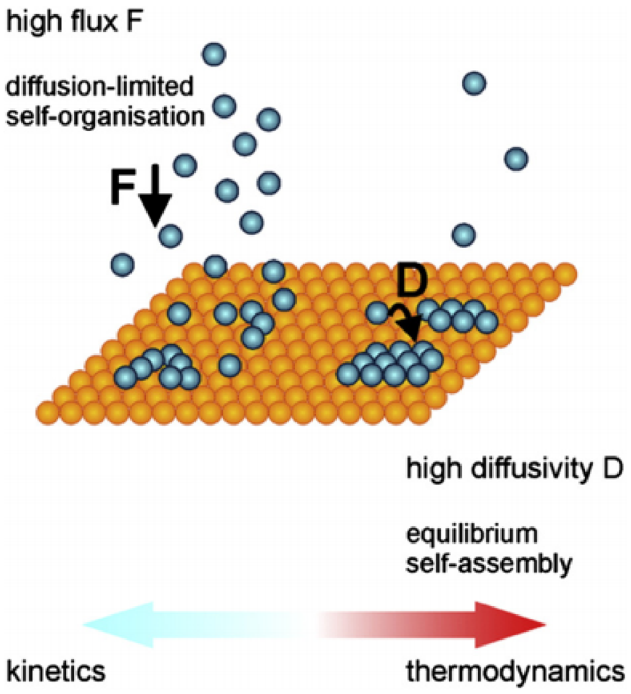

Figure 1.1: Schematic illustrating the difference between self-organization (left) and self-assembly (right). Molecules (blue) are deposited on a surface (yellow) with varying flux and diffusivity. On the left side a high flux of molecules but a low diffusivity is present resulting in self-organisation. On the right side a lower flux of molecules with a much higher diffusivity is present resulting in self-assembly. Adopted from [2].

that consists of many molecules. This situation is reversible, and until an equilibrium is found the molecules can freely diffuse around on the surface.

In order to tailor the self-assembly process, the different types of intermolecular interactions and interactions between molecule and substrate have to be considered. Table 1.1 gives an overview of which intermolecular interactions to take into consideration when either designing, or characterizing a self-assembled system.

Here, H-bonding, dipole-dipole and metal-complexation is indeed interesting when trying to tailor a self-assembly system due to their directional or selective nature.

Interactions between the molecule and substrate can be controlled by choice of substrate material but also the plane in which the single-crystal is cut. Due to their relatively inert nature the fcc packed Au, Ag and Cu are often chosen, listed in the order of least to most reactive. The crystal planes of said crystals also need to be taken into account.

Interaction type	Strength	Bonding length	Nature
van-der-Waals	∼0.1 eV	0.5-1 nm	Non-selective
H-bonding	0.1-0.5 eV	0.20-0.35 nm	Selective, directed
Electrostatic	0.1-3 eV	Up to several nm	Non-selective
Dipole-dipole	0.1-0.5 eV	0.2-0.3 nm	Directed
Metal complexation	1-3 eV	0.2-0.3 nm	Selective
Substrate-mediated	0.1-1 eV	up to 7 nm	Oscillatory
Reconstruction-mediated	1 eV	system dependent	Covalent

Table 1.1: Table with overview of the different interactions between molecules. The strength, bonding length and the nature of the interaction are listed to give an overview of what to consider when tailoring a self-assembled system. Adopted from [2].

Often the (111), (100) and (101) planes are chosen, listed in order of highest to lowest coordination number of the surface atoms in each plane. The higher coordination number of the (111) plane means less broken bonds of the surface atoms resulting in a less reactive surface.

1.2 VOPc and VOTTDPz Investigated on Metallic Substrates

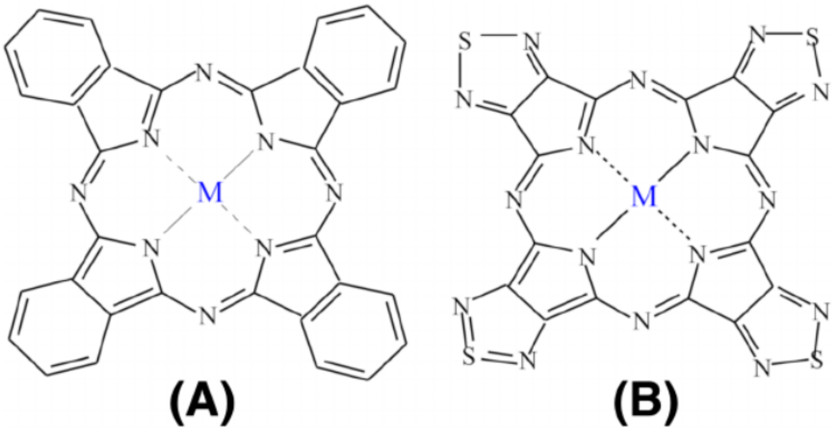

Figure 1.2: Schematic showing (a) Pc molecule supporting a metal center and (b) TTDPz supporting a metal center. Adopted from [3].

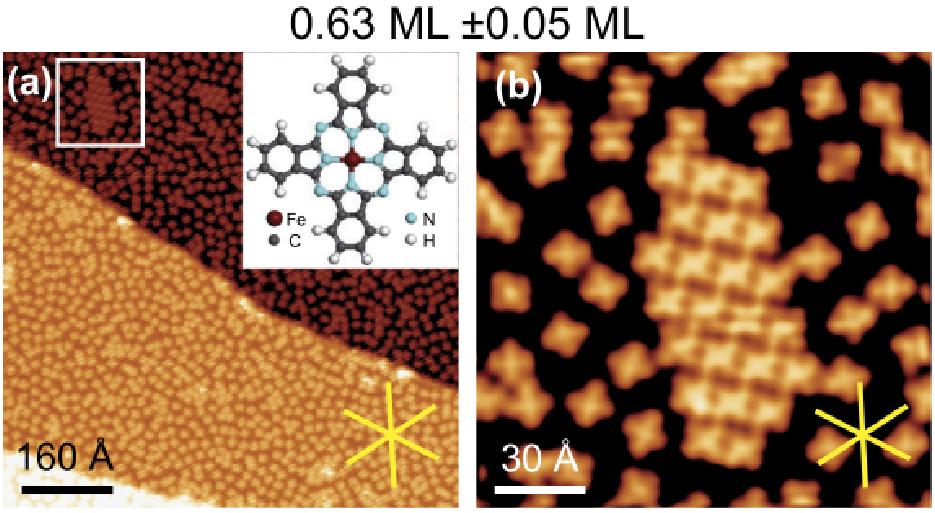

Figure 1.3: STM topography of 0.63 ML coverage of FePc on Cu(111). (a) 800×800 $Å^2$ overview showing individual adsorbates and smaller islands of FePc. (b) 150×150 $Å^2$ area taken from the indicated area of (a) showing in detail how the FePc molecules are oriented. The yellow star denotes the axes of the close packed Cu(111) surface. Adopted from [4].

1.2.1 Metal Phthalocyanines

Phthalocyanine (Pc) is one of the most well-studied organic molecules, since its discovery in 1928. As can be seen in Figure 1.2 (A) it is a planar aromatic macromolecules that consists of four isoindole units having an 18 π-electron delocalized electron cloud. Due to their thermal and chemical stability they have been studied intensively. A very interesting feature of these molecules is their ability to support metal centers in their central cavity. So far 70 different metals have been incorporated into Pc's, and this metal-organic complex has the term MePc's. The metal center is held in place by the four aza-bridging Nitrogen atoms, and the bonds involve charge transfer from the metal to the ligand, usually leaving the metal in a positive ionized state. Studies performed on FePc's by Snezhkova et al showed that when depositing these molecules onto a Cu(111) substrate by means of thermal evaporation the self-assembled structures were coveragedependent. At coverages of 0.5-0.65 ML isolated adsorbates where found, and only in the upper end of this range islands of adsorbates began forming. They attributed this to the molecule-substrate interactions dominating the intermolecular interactions. Furthermore they found that when the small islands of FePc formed, all of the molecules were oriented with one of the molecular axes oriented along a close-packed row of the Cu(111) surface, whereas the individual FePc-molecule adsorbed around the surface would orient themselves in a random manner. This is visualised in Figure 1.3. Visible in this figure is the distinct clover-like molecules, which is the case for all of the Pc's and their derivatives.

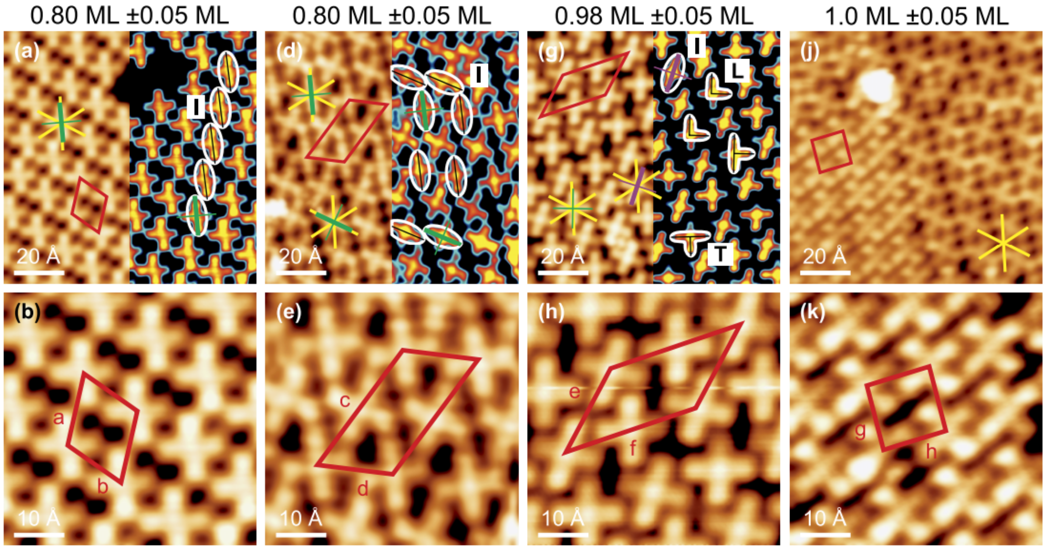

Figure 1.4: FePc coverage of 0.8 ML-1 ML. (a) one of two observed structures at 0.80 ML, and (b) the unit cell of the structure found in (a). (d) the second structure observed at 0.80 ML, and (e) the unit cell of structure found in (d). (g) structure found at 0.98 ML, and (h) its unit cell. (i) structure found at 1 ML, and (k) its unit cell. Yellow stars denotes the axes of the closed packed surface. Green and yellow crosses denotes the alignment of the FePc molecules. Adapted from [4].

An investigation of higher degrees of coverage from 0.80 ML-1 ML revealed highly ordered structures as can be seen in Figure1.4. At 0.80 ML coverage two different structures were observed. One structure (a) had all of the molecules aligned to one of the axes of the closed packed surface, whereas the other structure (d) had some of the molecules align after one axis, whereas the molecules in the adjacent row would be align along a different close-packed surface axis. It can be seen in (b), (e), (h) and (k) how the unit cell changes significantly with the varying structures, although the group found that the packing density of the molecules did not vary by much.

The effect of annealing the FePc/Cu(111) system was also investigated in this study. At a temperature 250°C lead to a well ordered structure as observed pre-annealing, but with a higher packing density. When heating to 300°C a loss of order in the structure was seen overall. Here indication of reactions between the adsorbates was also seen as the molecules were in direct contact with each other. They further theorized that the intermolecular bonds of the adsorbated changed nature, and a breaking of the π-bonds resulted in a stronger chemisorpt σ-bond to the Cu(111) substrate. Annealing a submonolayer near the sublimation temperature of FePc, 320°C, showed a reorganization of the individual adsorbed molecules into two kinds of alignment. One alignment was along one of the close packed surface axes, whereas the other deviated by -8°.[4]

Another study performed by Niu et al[5] of VOPc deposited onto Au(111), Ag(111) and Cu(111), revealed that adsorption both with the oxygen pointing out of surface plane (O-up) and into surface plane (O-down) were present on all of the different substrates and at all of the investigated degrees of coverage (from 0.2-1 ML VOPc). An example of such a mixture of O-up and O-down can be seen in Figure 1.5.

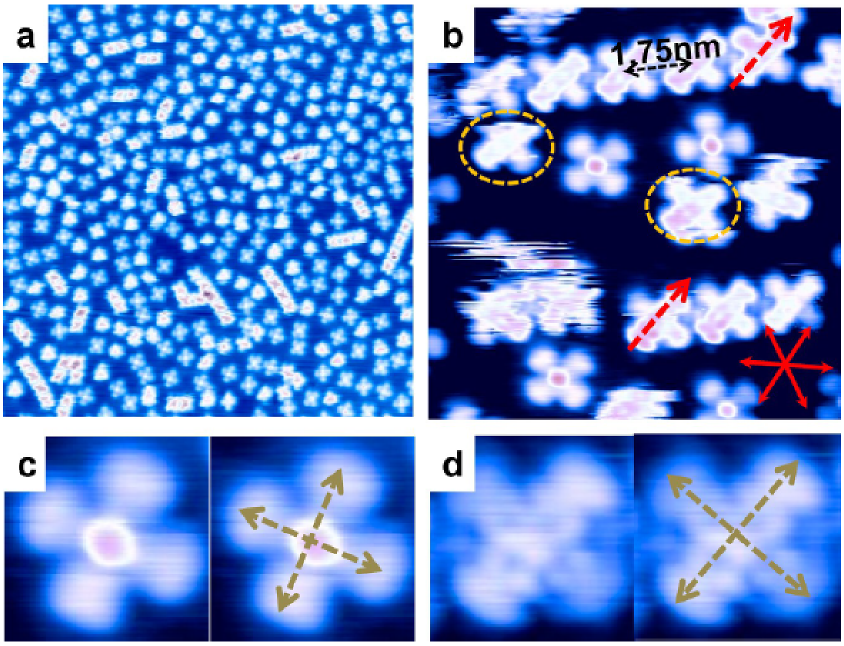

Figure 1.5: VOPc on Cu(111) at 0.2 ML coverage. (a) STM topography showing the random mixture of the O-up and O-down configuration of adsorped VOPc's. (b) a chain of VOPc consiting of both O-up and O-down VOPc's. The molecules in the chains are aligned along of the closed packed surface axes. (c) Enlarged topography of O-up configuration. (d) Topography of O-down configuration. Adopted from [5].

The distance between two neighbouring VOPc molecules in this chain-configuration was measured to be 1.75 nm from center to center.

Krull [6] investigated the magnetic and electronic properties of CuPc. He created a 3×3 cluster of CuPc molecules by laterally manipulating them with the probing tip - this assembly can be seen in Figure 1.6

Here it is seen how the dI/dV conductance maps vary greatly depending on which applied bias voltage was used. Especially interesting is how the LDOS visible changes depending on how many nearest neighbor (NN) molecules the different molecules have. This is especially visible at (d) where the corner molecules (2NN) appears as black circles, the molecule in the middle (4NN) is blue and the molecules in the sides (3NN) is yellow/orange. A visible change in the electron clouds are visible possibly due to the coordination-number of the molecules.

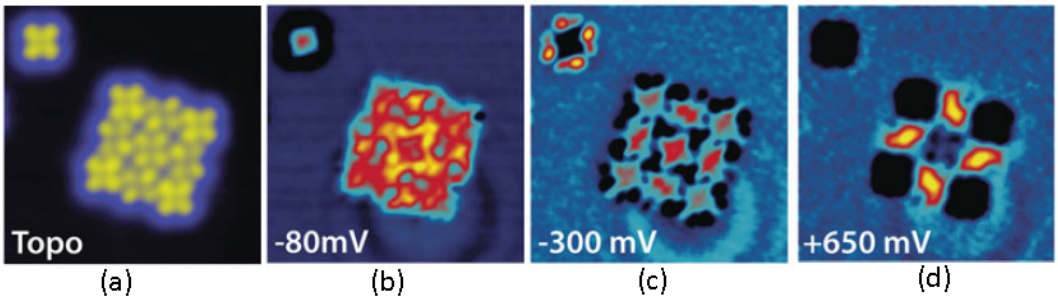

Figure 1.6: 3×3 cluster of CuPc molecules created by manipulating the molecules with the tip. (a) Topographic image of the cluster. dI/dV conductance map obtained at (b) -80mV, (c) -300mV and (d) +650 mV. Adapted from [**?**]

1.2.2 Metal tetrakis(thiadiazole) phorpyrazine

Tetrakis(thiadiazole) phorpyrazine (TTDPz) is a derivative of the Pc molecule. Instead of the aromatic ring in the isoindole group, TTDPz has four five-member rings terminated by Nitrogen and Sulfur. This type of molecule is relatively new, as it was first synthesized in 1996 by P.A. Stuzhin et al [7], but an interest in its properties has arisen. This is due to the replacement of the aromatic rings, that not only leads to a smaller molecule, but also replaces the relatively weak $C\cdots H$ termination which should lead to stronger intermolecular interactions due to strong side-by-side electrostatic attractive forces of $S\cdots N$ between adjacent MTDDPz molecules[7].

1.2.3 Vanadyl tetrakis(thiadiazole) phorpyrazine

A study performed by Miyoshi et al[8] synthesized and investigated two crystal forms, α (needle formed crystals) and β (block shaped crystals), of VOTTDPz. The α-form was seen at temperatures of growth at 380 $^{\circ}C$ and β was seen at temperatures above 400 °C. They found that the Vanadium ion was not in plan with the ligand, but was positioned 0.566 Å above, bound to the Oxygen ion with a bonding length of 1.609 Å, which is slightly longer than the usual Vanadyl-bond-length of 1.57-1.59 Å. Molecular orbital calculations suggests a V^{+4} $\left(d^1\right)$ groundstate.
The same study investigated the magnetic properties of the α and β crystal form, by means of a SQUID magnetometer, and the paramagnetic susceptibility, χ_p, was found and plotted in a $\chi_p T$ vs T plot as can be seen in Figure 1.7. Here it can be seen that the value of $\chi_p T$ differs significantly at low temperatures - the α-form has a much higher value at temperatures near absolute zero, than the β-form has. Furthermore a more linear tendency of the $\chi_p T$ value is seen for the β-form compared to the more exponential behaviour of the α-form.

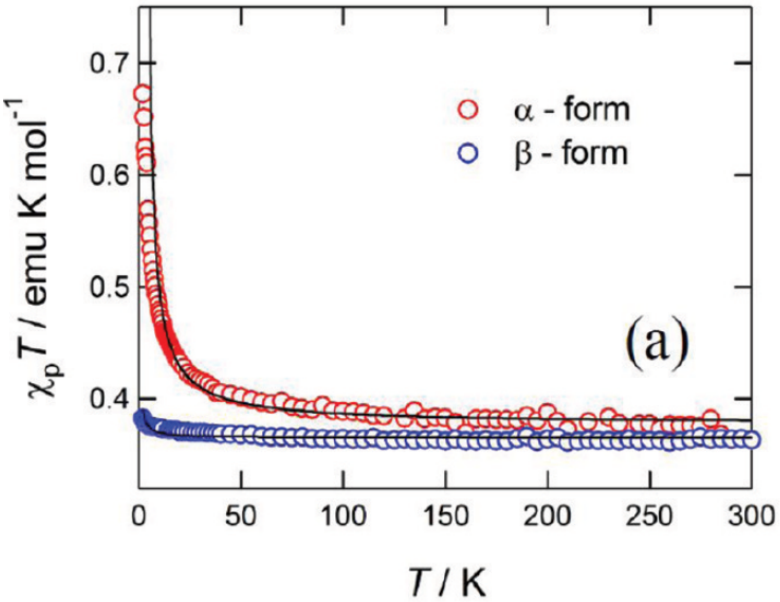

Figure 1.7: Temperature dependence of $\chi_p T$ as a function of T for the α- (red) and β-form (blue) of VOTTDPz. The solid black lines denotes the best fit to the data of the Curie-Weiss law. Adopted from [8]

To further investigate the electronic and magnetic properties of VOTTDPz, the study performed electron paramagnetic resonance (EPR) measurements on VOTTDPz diluted into a close-shelled compound, being H_2TTDPz in a ratio of 1:50 of VOTTDPz:H_2TTDPz. The plot of the data obtained by EPR can be seen in Figure 1.8.

VOTTDPz has an unpaired electron on the Vanadium metal center, and has 1/2 spin. Vanadium has a nuclear spin of 7/2. Therefore eight distinct peaks should be observed in EPR measurements. Miyoshi et al. found that the EPR-measurements of VOTTDPz was very much in agreement with the simulated hyperfine structure of $^{51}V^{4+}$, meaning that the unpaired electron of VOTTDPz is located around the Vanadium metal center. There was one peak noted with a star in Figure 1.8 that was not in agreement with the simulation - This peak Miyoshi et al. explained as a possible interference related to the aggrevated dilute, being H_2TTDPz.

Another study performed by Hou et al[9] investigated Vanadyl tetrakis(thiadiazole) phorpyrazine (VOTTDPz) on Au(111) as the more noble nature of Au compared to Ag and Cu should lead to a weaker substrate-molecule interaction and thereby the intermolecular interactions would be more prominent resulting in larger ordered networks of said molecule. The group deposited VOTTDPz by means of thermal evaporation at temperatures between 280-300°C onto Au(111) held at room temperature (RT) and subsequently performed STM measurements at liquid helium

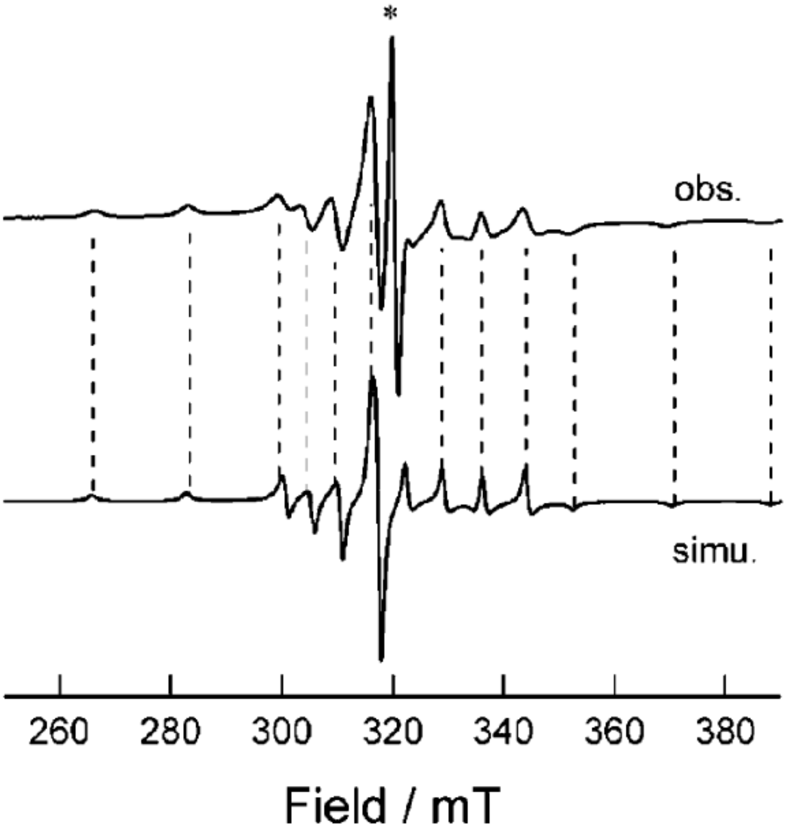

Figure 1.8: EPR spectrum of VOTTDPz diluted in H_2TTDPz (obs.), and simulated spectrum of hyperfine structure of $^{51}V^{4+}$ (simu.) with g_{xy}=1.982 and g_z=1.960. Intensity in arb. unit is plotted as a function of the magnetic field in mT. Adopted from [8]

temperatures (4.7 K).

As seen in Figure 1.9(b) a well ordered monolayer of VOTTDPz was achieved and successfully imaged by means of STM. The molecular structure is outlined in (a) with the oxygen pointing out of plane. Alternating bright and darker spots on each molecule is visible in (b) and is attributed to the O-up and O-down configurations respectively, by no apparent specific order, which is in agreement with [5]. In (c) the arrangement of individual molecules in the network can be seen. Here it is noteworthy that the molecules are rotated 30° with respect to each other, compared to the pattern found in the study of FePc on Cu(111) where the molecules arranged themselves after the axes of the close packed Cu(111) surface. This witnesses about a stronger intermolecular interaction which is also supported by the fact that the distance between VOTTDPz molecules were measured to 1.12 nm, which is smaller than the 1.44 nm measured for VOPc[**?**]. (d) shows the unit vectors s,t of the

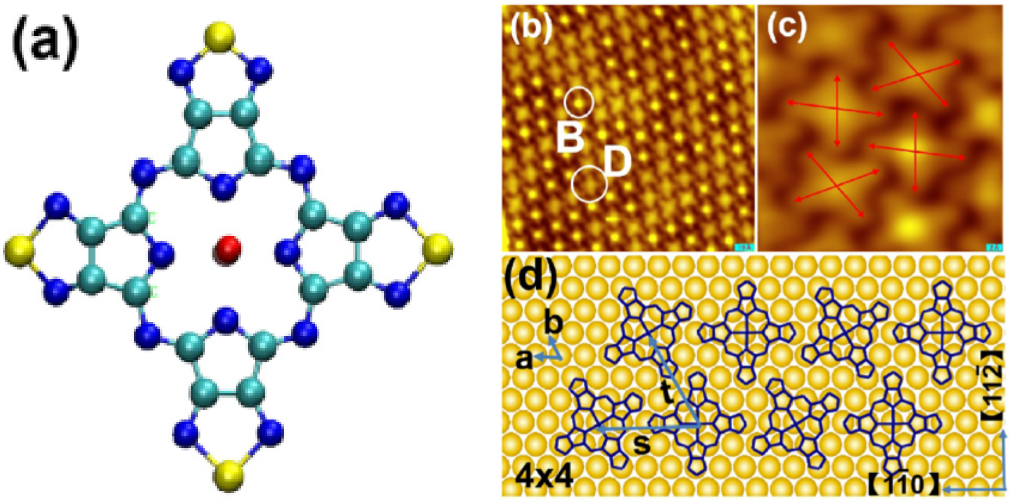

Figure 1.9: (a) Molecular structure of VOTTDPz with oxygen (red) pointing out of the plane. (b) 13×13 nm^2 topographic image of VOTTDPz monolayer taken by means of STM - The letters B and D denotes the O-up and O-down configuration respectively. V_{bias} = -0.8 V, I= 160 pA (c) 3×3 nm^2 detailed overview of the arrangement and rotation of the VOTTDPz molecules in a monolayer - the red crosses denotes the molecule-axes. (d) Schematic representation of the lattice of VOTTDPz-molecules. Visible in yellow is the Au(111) surface. s,t and a,b are unit vectors of the molecule-lattice and Au(111)-lattice respectively. Adopted from [9]

molecules, and a,b of the Au(111) surface. The unit vectors s, t of the molecules can be expressed in the following way by means of the Au(111) unit vectors:

$$\begin{pmatrix} s \\ t \end{pmatrix} = \begin{pmatrix} 4 & 0 \\ 0 & 4 \end{pmatrix} \begin{pmatrix} a \\ b \end{pmatrix} \tag{1.2}$$

The nearest-neighbor-distance between VOTTDPz molecules was as mentioned measured to be 1.12 nm (4 times that of the interatomic distance of the Au(111) substrate).

Chapter 2

Methods and Experimental Setup

2.1 Experiments Performed at the University of Copenhagen

In order to study the chemical and magnetic properties of the synthesized VOTTDPz a series of experiments were carried out at the University of Copenhagen in collaboration with Professor, Jesper Bendix, whom had synthesized the VOTTDPz used in this project. The following experiments were carried out from the 19th of October till the 22nd of October 2020.

2.1.1 Powder X-ray Diffraction

VOTTDPz was investigated by means of Powder X-ray Diffraction (PXRD) and were recorded at room temperature using a Bruker D8 ADVANCE powder diffractometer operating in a $2\theta - \theta$ configuration using CuK_α radiation (λ = 1.5418 Å). Powder samples were dispersed on a zero background holder of Si wafer cut parallel to 511 fastened on a poly(methyl methacrylate) sample holder. The powder patterns were simulated in Mercury without inclusion of preferred orientation effects.

2.1.2 Electron Paramagnetic Resonance

Electron Paramagnetic Resonance (EPR) was recorded with a Bruker Elexsys E500 equipped with a Bruker ER 4116 DM dual-mode cavity, an EIP 538B frequency counter an ER035M NMR Gauss meter, and an Oxford Instruments iTC cryocontroller. The spectra were recorded at X-band frequencies (ν ≈9.63 GHz) in DMSO solution in glass capillary tubes. The spectra were simulated using home-written software (H. Weihe, Univ. of Copenhagen) considering an electronic spin of S=1/2 and taking into account only the experimentally resolvable interactions with the nuclear spins of one vanadium-51 (I=7/2).

2.1.3 Magnetic Measurements

Magnetic measurements were recorded using a Quantum Design MPMS-XL SQUID magnetometer equipped with a 5 T dc magnet on a polycrystalline sample consisting of 8mg of VOTTDPz powder packed in a polycarbonate capsule. The susceptibilities were corrected for diamagnetic contributions from the sample holder and the constituent atoms by means of the measured diamagnetism of the sample holder and an estimate of the diamagnetism of the constituent atoms.

2.2 The Ultra High Vacuum System and Preparation of Samples

2.2.1 The Ultra High Vacuum System

For the STM to function optimally and to obtain the best possible scans, an ultra clean environment is necessary, since even a speck of dust can ruin the contour of the surface. One way to ensure the best possible conditions for operating the STM is by encasing the microscope in ultra high vacuum (UHV). UHV conditions are fulfilled when a base pressure of 10^{-8}mbar-10^{-12}mbar is reached. The UHV system used in this study consists of three compartments separated by sealing shutters to ensure stable independent pressures in each compartment. The compartments and their function are as follows:

- Loadlock: The loadlock is used to transfer samples into the UHV-system by means of a wobble-stick. Since this chamber is the access-point to the UHV-system, and its major function is to hold and transfer samples, it can operate under the highest pressure in the system. Two pumps are connected to the loadlock ensuring that the pressure can be lowered from atmospheric to UHV conditions. A membrane pump lowers the pressure from atmospheric pressure to 0.1mbar. At this point in pressure a turbo-molecular pump takes over and pumps the loadlock to a pressure of 10^{-10}mbar.

- Preparation chamber: In the preparation chamber a base pressure of 10^{-10}mbar-10^{-11}mbar is reached by an Ion Getter Pump. In the preparation chamber a manipulator with different preparation stations is utilized. In this specific study a heating station has been used when cleaning the samples as well as an Ar sputter source. Furthermore molecular beam evaporators connected to the preparation chamber has been utilized to deposit the investigated molecules onto the metal samples.

- STM chamber: The STM chamber has a base pressure of $4 \cdot 10^{-11}$mbar which is reached by another Ion Getter Pump connected directly to the chamber. Two cryostats are in the chamber ensuring that the STM can operate under low temperatures. In this study both chambers were filled with liquid nitrogen with a temperature of 70K measured on the inner cryostat, but the smaller inner cryostat can be filled with liquid helium as well, ensuring temperatures around 10K.

To decouple the STM from the rest of the system and to thereby isolate it from external vibrations of the surroundings a spring mechanism is used, suspending the STM when scanning.

Furthermore the UHV-chamber is placed on a concrete block separated from the rest of the building, to eliminate vibrations from the surrounding room. To support the UHV-chamber laminar flow stabilizers are used. These stabilizers further dampen the vibrations as well as keeping the UHV-chamber level.

2.2.2 Sample Cleaning Process

In order to get a clean sample before the deposition of the investigated molecules, the sample needed to undergo a cleaning process. In this study the process consisted of an Ar sputtering to get rid of impurities and subsequently an annealing of the sample to let the atoms of the substrate recrystallise as well as removing residual impurities. The sputtering process was performed under a base pressure of $3 \cdot 10^{-6}$mbar by letting in Ar gas in the preparation chamber till this pressure was reached. During the sputtering the Ar sputter source was kept at an energy of 1keV and the sample was sputtered for 25 minutes consistently. The annealing of the sample was performed by placing the sample in a heating stage on the manipulator in the preparation chamber and by resistive heating achieving a temperature of 640-660○C measured on the heating stage. At this temperature the sample was kept for 5 minutes, and subsequently cooled down very slowly to ensure large flat terraces of the surface.

In order to get a sample clean enough for optimal scanning, 2-3 cycles of sputtering and annealing was performed in between measurements.

2.3 Deposition of Molecules

2.3.1 Preparation of Molecules before Deposition

In order to deposit the investigated molecules onto the substrate effusion evaporation was performed by means of evaporation from a Knudsen Cell. The molecules investigated was in an amorphous powder form when delivered. Empty quartz cells were loaded into an OMBE molecule evaporator that was subsequently attached to the preparation chamber separated with a valve ensuring no contaminants leaking into the preparation chamber. The molecule evaporator was then heated to a temperature of 130°C in order to remove contaminants and water since

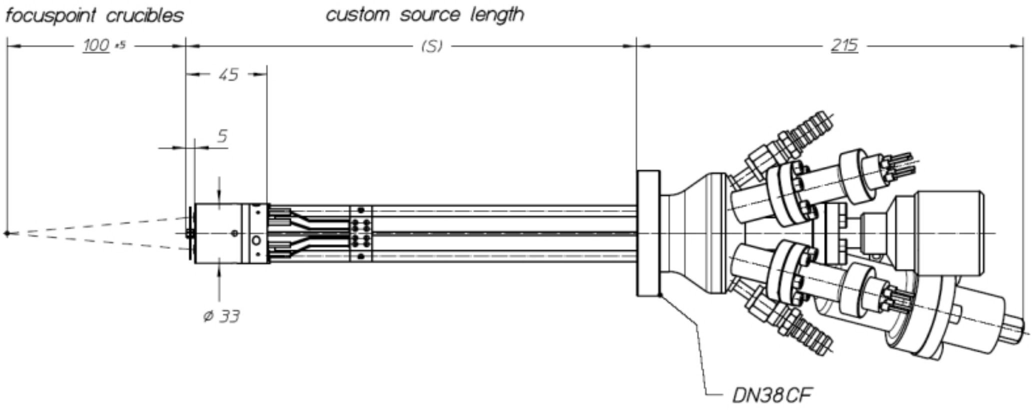

Figure 2.1: Schematics showing the OMBE molecular evaporator. Focal point of the molecule-beam is 100 mm. Adopted from [10]

the quartz cells had been kept under ambient conditions. A tube running up to the loadlock was opened during the heating so the turbomolecular and membrane pump could remove any contaminants. After heating the quartz cells overnight the molecule evaporator was detached from the preparation chamber and the molecules in powder form was loaded into the quartz cells. Before deposition of the molecules, the cell containing VOTTDPz was heated to 250°C and kept at this temperature for 5 hours. A shutter was opened, so the turbopump and membrane pump could remove the excess gas generated from the heat. Subsequently the shutter was closed, and the shutter between the OMBE evaporator and the preparation chamber was opened, allowing the molecules to be deposited onto the substrate in question.

Schematics delivered with the OMBE molecule evaporator indicated that the ideal placement of the sample for a focal point of evaporated molecules to hit was 10cm from the evaporator as seen in Figure 2.1. The molecule evaporator was adjustable and was placed at an approximate distance of 10cm from the sample located on the manipulator in the preparation chamber.

A molecule (VO-salen) with a known sublimation temperature (250 °C) was chosen to calibrate the position of the OMBE evaporator. The calibration was done bye having the OMBE evaporator in a certain distance (z-position) from the sample (Au(111), deposit VO-salen at 250 °C for 15 minutes, and investigate if molecules were visible on the substrate. If no molecules were present, the z-position would be adjusted, and a new deposition would be performed. The initial z-position was 10, but after adjusting the z-position ended up at 0 (closer to the sample). The result of a deposition of VO-salen at this z-position can be seen in Figure 2.2

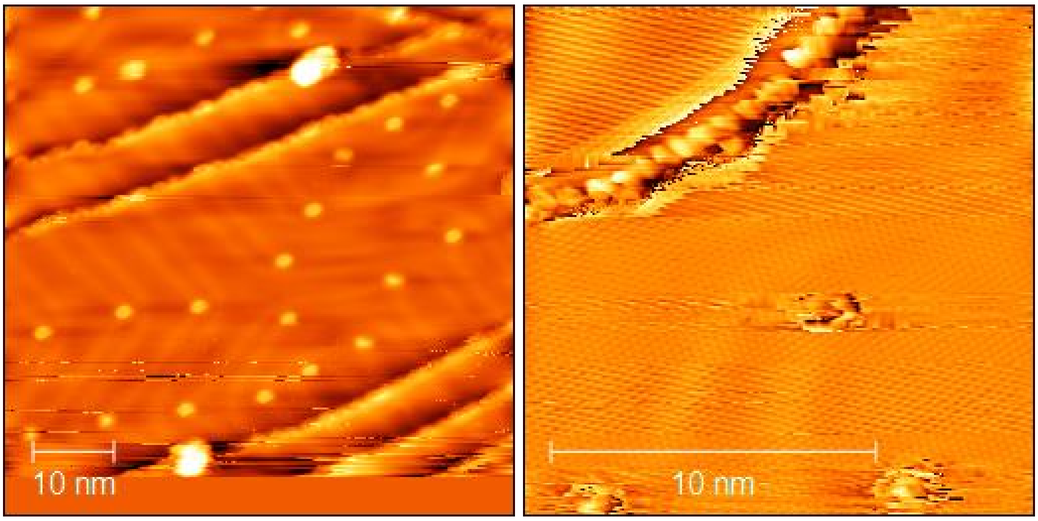

(a) (b)

Figure 2.2: (a) The Au(111) surface after deposition of VO-Salen at z-position 10. No molecules are visible (b) The Au(111) surface after deposition of VO-salen at z-position 0. Drift is apparent, and what appears to be ordered structures are seen covering the whole investigated area.

After the deposition at z-position 10, the sample was investigated, and the result can be seen in Figure 2.2a. The bare Au(111) surface is seen, and no molecules are visible. Therefore the z-position was adjusted, and at z-position 0, the result after deposition of VO-salen can be seen in Figure 2.2b. Here a distorted image influenced by drift can be seen, as well as what appears to be ordered structures covering the whole investigated area. Initially this structure was believed to be VO-salen covering the whole surface, and subsequently the z-position was held at 0 for the remaining depositions.
After adding a scale-bar to the investigated area, it though became apparent that the size of the individual features of the ordered structure was too small to be those of VO-salen. This is visualized in Figure 2.3.

Here the individual features appear to be approximately 0.3 nm in size, which could be indicative of the image showing atomic resolution of Au(111). To confirm this suspicion a line was drawn through the centers of 10 individual features, and the distance measured was 2.84 nm. This corresponds very well with the interatomic distance between individual Au-atoms of the Au(111) being 2.884 Å [11].

2.3.2 Deposition of VOTTDPz

A study performed by Hou et al [?] had found that an evaporation temperature of 280-300°C from a Knudsen Cell yielded self assembled structures of VOTTDPz molecules on a Au(111) surface under UHV conditions. In order to be safe and not

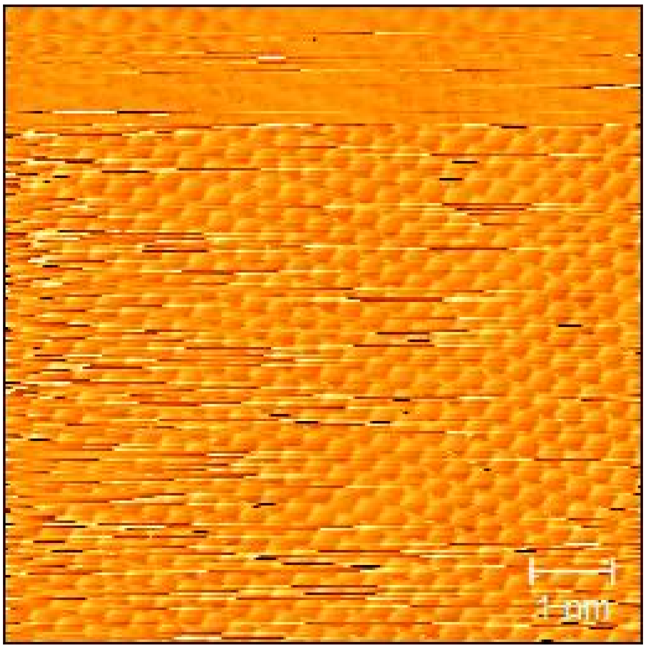

Figure 2.3: A 78Åx78Å image of the Au(111) surface taken in the investigated area after depositing VO-salen at a OMBE z-position of 0. Ordered individual features can be seen. A scale-bar of 1 nm is imposed in the lower right corner.

heat the molecules to a temperature, that could break them, an initial thermogravimetric analysis (TGA) was performed on the pure VOTTDPz powder. A platinum boat was filled with VOTTDPz powder, and heated from 100 °C to 500 °C using a Thermogravimetric Analyzer from TA instruments. The mass of the powder was measured as a function of temperature and can be seen in Figure 2.4.

In order to see the change in weight as a function of temperature, the first order derivative of the weight as a function of temperature was plotted. This can be seen as the green line in Figure 2.4. Since the aforementioned study used a deposition temperature in the range of 280-300°C the peaks of the TGA was investigated near this range. A peak around 265 °C can be seen, and therefore a temperature of 250 °C was chosen for the initial depositions and subsequently temperatures of 260 and 270 °C was used as deposition temperatures, the latter being used consistently hereafter. Large peaks can be seen from around 300 °C and onwards, and was speculated to be due to the molecules breaking which is why a relatively low deposition temperature was chosen for the initial depositions.

2.3.3 Annealing after Deposition of VOTTDPz

After deposition of VOTTDPz and initial STM investigations both the VOTTDPz/Au(111) and VOTTDPz/Ag(111) systems were annealed in order to see if addition of ther-

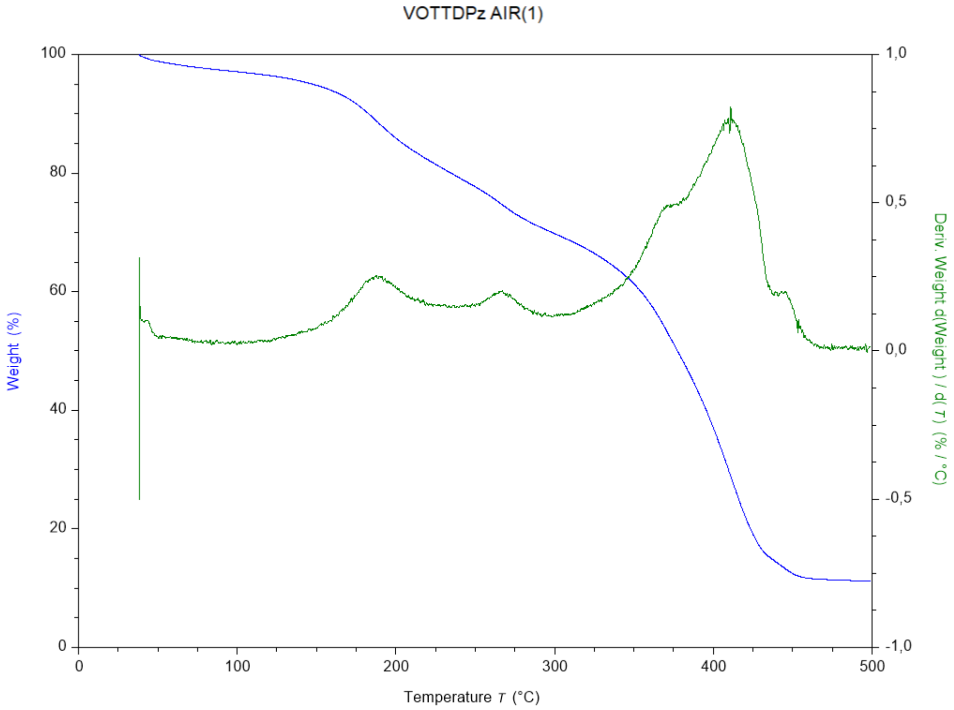

Figure 2.4: Data from TGA performed on VOTTDPz. The blue line denotes the weight of VOTTDPz as a function of the temperature. The green line denotes the first derivative of the weight with respect to temperature.

mal energy would result in rearrangement of the adsorbed species. The annealing temperatures were 54 and 74 °C measured on the thermo-couple placed on the heating-stage. The duration of the annealing was set at 5 minutes from reaching the desired temperature. The relatively low annealing temperatures compared to the sublimation temperature of VOTTDPz was chosen in order to not alter the molecular structure by for example breaking bonds.

2.4 The Scanning Tunneling Microscope

[12] The Scanning Tunneling Microscope used in this project utilizes a W tip which is attached to a piezodrive. Here three mutually perpendicular piezo-transducers named the x-, y- and z-piezo is used to probe the surface investigated. A saw-tooth voltage is applied to the x-piezo and a voltage ramp is applied to the y-piezo leading to the tip scanning the xy-plane. With an applied bias-voltage the z-piezo is then brought close to the surface of the substrate (a few ångströms from the surface). At this distance the electron wavefunctions of the sample and the tip overlaps, and the applied bias-voltage results in a current flowing between tip and

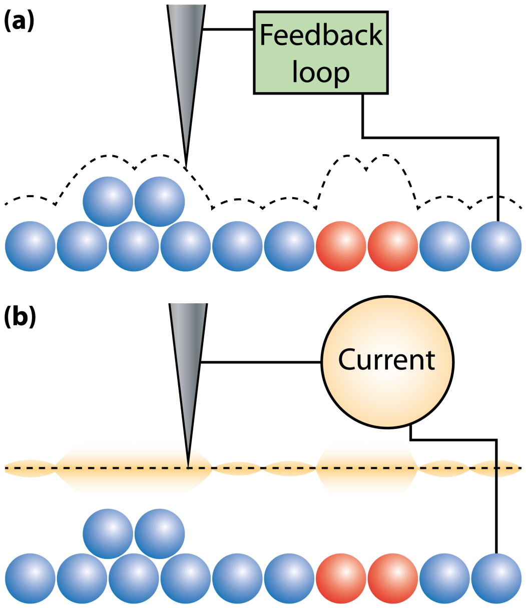

Figure 2.5: Schematic showing (a) constant current mode and (b) constant height mode. The red atoms have a different apparent height than the blue. Adopted from [13].

sample or vise versa. This current can be described as quantum mechanical tunneling which will be described later. The current flowing between tip and sample is amplified and converted to a voltage which is compared to a reference voltage. Typically a negative feedback loop is employed, meaning that if the current flowing is greater than the reference-value, the z-piezo will retract the tip from the surface. This mode is called constant current mode, since the feedback system ensures that a constant current is flowing between the tip and sample and is the most commonly used mode, since it prevents the tip from crashing into the surface. The retraction of the tip is then converted to an output. If a very flat surface is scanned the constant height mode can also be employed. Here the tip is held fixed at a certain height above the surface, and the varying current is then the output. Both modes are depicted in Figure 2.5.

Here it is noticeable that even though the red and the blue atoms are the same size, the red atoms has a different apparent height than the blue atoms, due to differences in the local density of states.

2.5 Tunneling Theory

If considering a particle with a certain energy in the vicinity of a potential barrier, whose potential is higher than that of the particle, there would by a classical mechanic description be no chance of the particle crossing the barrier. If looking at a sufficiently small system, which has to be described quantum mechanically, the story is different. Quantum mechanics rely heavily on particle/wave-duality - that is matter can both behave as a particle, but also as a wave. This leads to a given uncertainty when either measuring the momentum or the position of said particle - if the momentum is very well defined, the position cannot be measured, and vice versa - this is called the Heisenberg uncertainty principle. Hence the probability of the particle crossing the potential barrier is no longer zero, but instead decays exponentially over the width of the barrier. That said the probability is dependent on the height of the potential barrier, as well as the width.

This mechanism is utilized in the STM, where a sharp well-defined probing tip, with ideally one apex-atom, is positioned a few Å from a sample. The tip-sample distance is exactly the width of the potential barrier. In order to understand the mechanism of tunneling utilized in the STM, firstly a simple 1-dimensional time-independent description will be given, where-after a more realistic 3-dimensional description that also takes the electronic structure of tip and sample into account is presented.

2.5.1 1-dimensional Time Independent Model

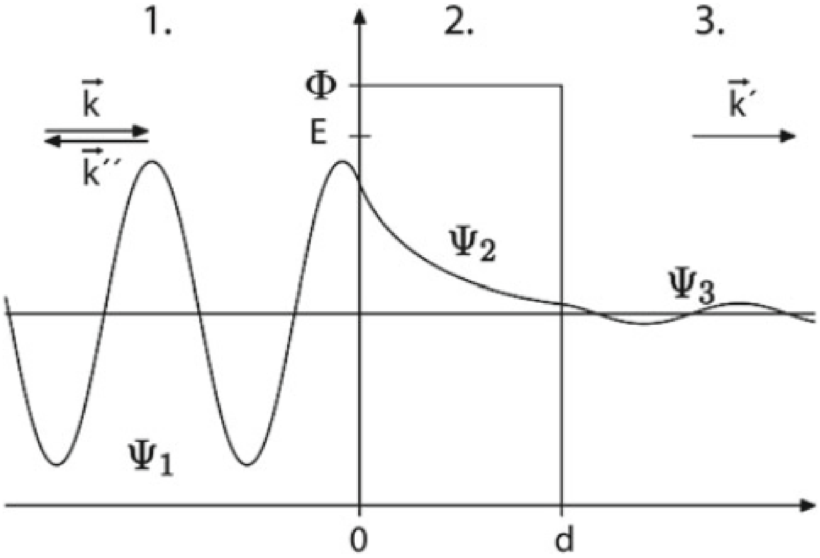

Figure 2.6: A one-dimensional potential barrier with height Φ and width d. The particle moving from left to right undergoes three regions, described by three different wave-functions: Ψ_1 (before barrier), Ψ_2 (inside the barrier) and Ψ_3 (after the barrier) leading to three different wavenumbers: $\vec{k}$, $\vec{k}'$ and $\vec{k}''$. As can be seen, it is the $\vec{k}'$ solution that crosses the barrier. Adopted from [**?**]

A free electron with energy E and a potential barrier with height Φ and width

d is used in this model. The time independent Schrödinger equation (Eq 2.1) has to be solved for the wavefunctions of the tip, sample and barrier.

$$\left(\frac{\hbar^2}{2m_e}\Delta + V(r)\right)\Psi = E\Psi \tag{2.1}$$

Here m_e is the electron mass, $V(r)$ is the potential of the barrier, and E is the energy of the electron. Assuming a plane wave anzats the solution for the wave functions can be found analytically in the three regions - namely tip (before barrier), vacuum (inside barrier) and sample (after barrier).
The plane wave anzats gives rise to the tree following wave functions, one in each region:

$$\begin{aligned}\Psi_1 &= e^{ikz} + A \cdot e^{-ikz}\\ \Psi_2 &= B \cdot e^{i\kappa z} + C \cdot e^{-i\kappa z}\\ \Psi_3 &= D \cdot e^{ikz}\end{aligned} \tag{2.2}$$

Having $k = \frac{\sqrt{2m_eE}}{\hbar}$ and $\kappa = \frac{\sqrt{2m_e(\Phi - E)}}{\hbar}$

Solving for the coefficients A, B, C and D can be done by matching of the amplitudes and the first derivatives at the boundaries of the potential regions.
A transmission coefficient is then defined as the relationship between the square of the wavefunctions on both sides of the barrier. The definition looks as the following:

$$T = \frac{|\Psi_1|^2}{|\Psi_3|^2} = \frac{A^2}{D^2} = \left[\left(\frac{k^2+\kappa^2}{2k\kappa}\right)^2 sinh\left(\kappa d\right)\right]^{-1} \tag{2.3}$$

Assuming a high barrier potential compared to the electron energy, $\Phi >> E$, meaning $\kappa d >> 1$ leads to the following simplification of the transmission coefficient, T:

$$T \approx \frac{16k^2\kappa^2}{\left(k^2+\kappa^2\right)^2} \cdot e^{-2\kappa d} \tag{2.4}$$

As the transmission coefficient shows the fractions of electrons crossing the barrier, the tunneling current is proportional to the coefficient:

$$I \propto T \propto e^{-2\kappa d} \tag{2.5}$$

This reveals that the tunneling current is exponentially dependent on the tip sample distance. A change of 1 Å in sample-tip distance results in a change of the tunneling current by one order of magnitude, which supports why the STM has such high lateral resolution.

2.5.2 3-dimensional Tershoff-Hamann Model

A more realistic approach to describing the tunneling mechanism was proposed by Tershoff and Hamann in the 1980s. With an onset in the first-order perturbation theory developed by Bardeen in 1960 [14]. The model proposed by Bardeen looked at the tunneling matrix $M_{\mu,\nu}$ representing the overlap of the wavefunctions of the tip, Ψ_μ, and of the sample, Ψ_ν.

In this model the tunneling current for a general geometry expressed as seen in Eq 2.6

$$I = \frac{2\pi e}{\hbar} \sum_{\mu,\nu} f\left(E_\mu\right)\left[1 - f\left(E_\nu + eV\right)\right]\left|M_{\mu,\nu}\right|^2 \delta\left(E_\mu - E_\nu\right) \tag{2.6}$$

A more lengthy derivation performed by [**?**], but not presented here, found that when assuming low temperatures and low applied bias voltage, the work functions of the tip and sample being equal and the tip being modelled as a spherical potential (s-wave function) at the point closest to the surface, the expression for the tunneling current can be written as:

$$I \propto \frac{1}{V_{tip}} \sum_{\mu,\nu} \left|\Psi_\nu\left(\vec{r_0}\right)\right|^2 \delta\left(E_\mu - E_F\right) \delta\left(E_\nu - E_F\right) \tag{2.7}$$

This expression can be simplified when realising that the local density of states for tip and surface is defined in the following way:

$$\begin{aligned} \rho_{tip}\left(E\right) &= \frac{1}{V_{tip}} \sum_{\mu} \delta\left(E_\mu - E\right) \\ \rho_{surface}\left(E, \vec{r_0}\right) &= \sum_{\nu} \left|\Psi_\nu\left(\vec{r_0}\right)\right|^2 \delta\left(E_\nu - E\right) \end{aligned} \tag{2.8}$$

Inserting this into the expression for the tunneling current gives:

$$I \propto V \rho_{tip}\left(E_F\right) \rho_{surface}\left(E_F, \vec{r_0}\right) \tag{2.9}$$

Thereby the tunneling current depends on the LDOS as well as the tip position at the Fermi-Energy, E_F, meaning that the STM images the LDOS rather than the actual position of the atoms.

A more realistic approach to calculating the tunneling current is done by integrating over the states contributing to the tunneling current. Here the DOS of the tip and surface withing a finite range of bias-voltages. The tip-sample distance, d, the energy E of each state and the bias-voltage are all taken into account by the transmission coefficient $T\left(d, \epsilon, eV\right)$, and results in the following integral:

$$I \propto \int_{E_f}^{E_F+eV} \rho_{surface}\left(E_F - eV + \epsilon\right)\rho_{tip}\left(E_F + \epsilon\right)T\left(d, \epsilon, eV\right)d\epsilon \tag{2.10}$$

2.5.3 Scanning Tunneling Spectroscopy

Another key feature that is possible with the STM is scanning tunneling spectroscopy. Here the tip is positioned over a point of interest on the surface, whereafter the feedback loop is opened, thus leaving the tip held in a fixed position at a certain distance above the surface. Then a chosen range of applied voltages is swept through, and the subsequent tunneling current between tip and sample is obtained. Taking an onset in Eq 2.10 the differential conductance, $\frac{dI}{dV}$ can be approximated as:

$$\frac{dI}{dV} \propto \rho_{surface}\left(E_F - eV\right) \cdot \rho_{tip}\left(E_F\right) \tag{2.11}$$

assuming that the transmission coefficient, T, and the DOS of the tip, ρ_{tip} is constant in the chosen energy-interval. It can be seen that the differential conductance is directly proportional to the LDOS of the sample at the position of the tip.

2.5.4 Surface States of the Ag(111) and Au(111) Surfaces

In order to test the quality of the probing tip in regards to spectroscopy, a reference spectra of a well known surface was performed in this project. Ag(111) and Au(111) has well defined spectra for the surface states existing on these substrates. A surface state exist because of broken bonds on the surface in the termination of the bulk phase. These states cannot propagate into the bulk crystal, and they cannot propagate out into the vacuum. Hereby the states exists in form of a two dimensional confinement on the surface of the substrate.

A study performed by Kliewer et al [**?**] found distinct peaks in STS spectra attributed to the surface states found on Au(111), Ag(111) and Cu(111), which can be seen in Figure 2.7:

The spectra from Ag(111) and Au(111) was used as a guide in this project, in the regard that before every STS measurement performed on VOTTDPz, a spectra of the surface states were obtained first. For the Ag(111) surface such a reference spectra was not successfully attained.

On the Au(111) surface the prominent peak around -400 to -500 mV was found several times. An example of this is seen in Figure 2.8:

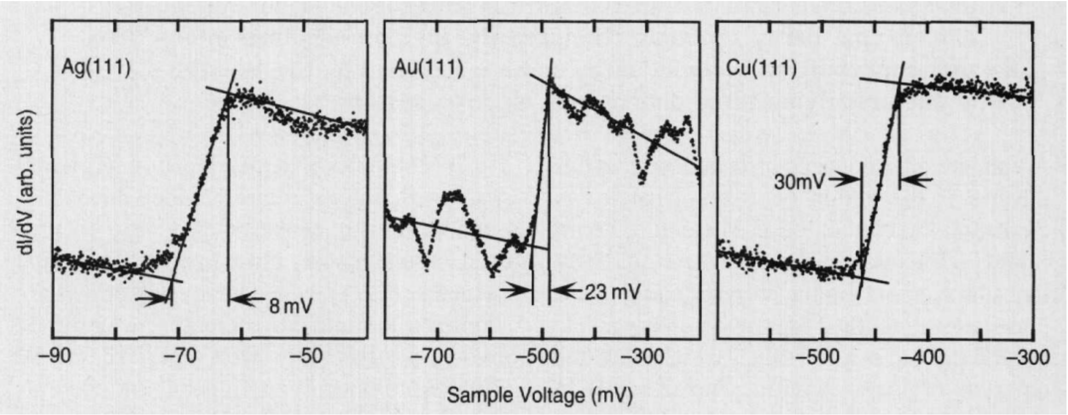

Figure 2.7: dI/dV spectra of Ag(111), Au(111) and Cu(111) from left to right. Adopted from [**?**]

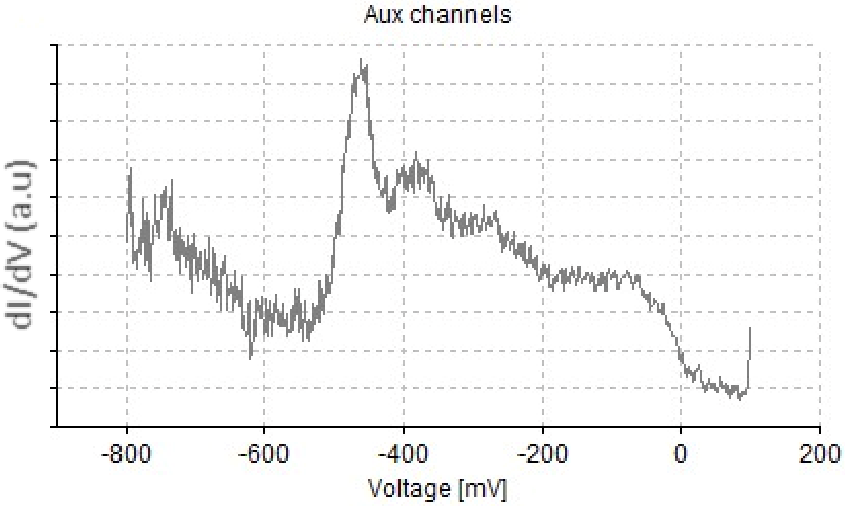

Figure 2.8: Reference spectra obtained on Au(111) surface between two of the lines of the herringbonestructure. A prominent peak between -500 and -400 mV is seen.

Chapter 3

Results and Discussion

3.1 Results Obtained from Experiments Carried out at the University of Copenhagen

The experiments performed on the synthesized VOTTDPz at the University of Copenhagen (KU) were carried out in order to investigate the composition of the VOTTDPz-powder, as well as to investigate the magnetic and electronic properties hereof.

3.1.1 Powder X-ray Diffraction performed on VOTTDPz

The synthesized VOTTDPz was investigated by means of PXRD. The measurement was run for 12 hours and plotted against simulated graphs of the α- and β-form as seen in Figure 3.1.

The black graph shows the experimental data obtained at the experiments run at KU, whereas the red and blue graph shows the simulated PXRD spectrum of the α- and β-crystal structure of VOTTDPz. It is noteworthy that peaks of both crystal-forms can be seen in the experimental data, although a clear tendency towards the β-phase is seen at the large peak around 27◦. The powder can therefore be a mixture of both phases, although the β-phase is more prominent as will be revealed later. The similarity between the experimental data and the simulated is also indicative of the powder actually being VOTTDPz. No visible crystals were seen in the powder, witnessing of an amorphous sample.

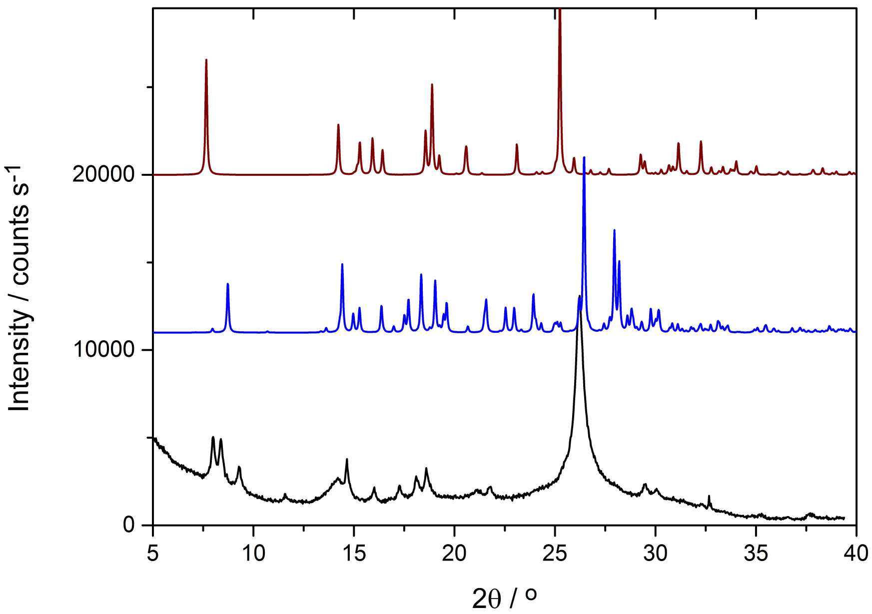

Figure 3.1: The experimental PXRD data obtained at KU on synthesized VOTTDPz used in this project (black) plotted against simulated PXRD plots of α (red) and β (blue) crystal forms. On the y-axis the intensity in counts per second is plotted against double the incident angle of light.

3.1.2 Electron Paramagnetic Resonance performed on VOTTDPz in DMSO solution

A solution of DMSO and VOTTDPz was made in order to carry out the EPR-measurements. The spectra was recorded at X-band frequency at $\nu \approx 9.63$ GHz. The field was varied from 2800 Gauss to 4400 Gauss, since the features of interest was found in this range, which was realised by running a few test runs initially. A simulation of the hyperfine structure of $^{51}V^{4+}$ was run on software written by H. Weihe. Here the temperature was set at RT (293 K), the frequency was set at ν = 9.6364 GHz, the g-factor at 1.966 and a Lorentzian bandshape. The data obtained experimentally was plotted against the simulation, and can be seen in Figure 3.2

Here it is evident, that the experimental data is highly in agreement with the simulation, as to both the positioning of the peaks as well as the intensity hereof. A slight "twisting" of the experimental graph could be explained by interference of VOTTDPz, that has not been diluted and hence interferes with the unpaired electron of other VOTTDPz-molecules. A g-factor of 1.96364 was used in the simulation to fit it properly to the experimental data, in agreement with Smith et al.[15] who states that the g-factor typically is around 1.95 for vanadyl. The very close similarity between the experimental and simulated data indicates the unpaired electron being located on the vanadyl-group in VOTTDPz.

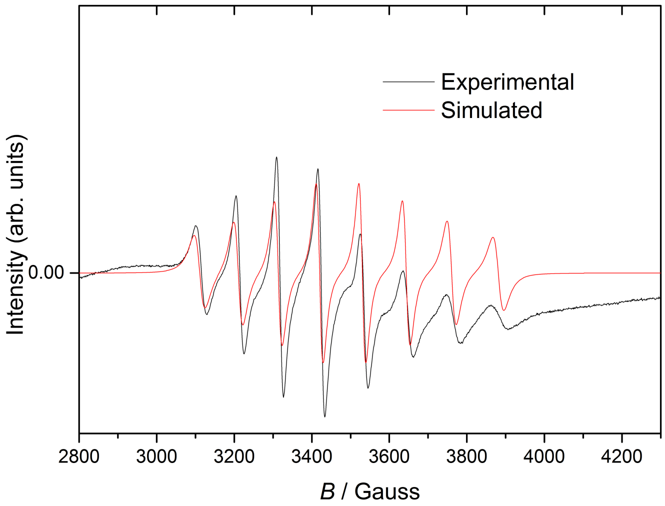

Figure 3.2: Experimental (black) EPR spectrum of VOTTDPz diluted in DMSO and simulated (red) EPR spectrum of $^{51}\text{V}^{4+}$. 8 prominent peaks are seen in agreement with a 1/2 spin system with a single nuclei having nuclear spin, I=7/2.

3.1.3 Magnetic Measurements

Miyoshi et al. found a distinct difference in the paramagnetic susceptibility, χ_p, between the two crystal forms, α and β as mentioned in Section 1.2.3. To investigate the magnetic properties of the VOTTDPz used in this project, magnetic measurements was performed using a SQUID-magnetometer. Here χT was plotted as a function of the temperature, and can be seen in Figure 3.3.

Here it can be seen that the plotted points follows an almost linear tendency, and that χT has an almost constant value of around 0.28. The linear tendency is in agreement with the data and fit found for the β-phase found by Miyoshi et al. Though they found the χT value to be a bit higher starting at around 0.4 and subsequently falling to around 0.35 as can be seen in Figure 1.7. The difference between the value obtained in the experiment carried out in this rapport and that found by Miyoshi et al. could be explained by a fault when weighing the VOTTDPz used in this project.

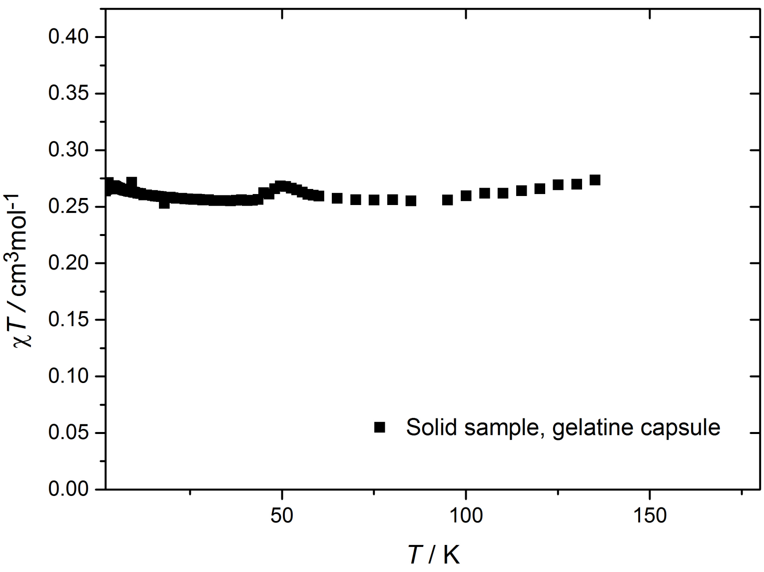

Figure 3.3: χT of VOTTDPz used in this project plotted as a function of temperature.

3.2 VOTTDPz deposited on Au(111)

3.2.1 Deposition after Degassing

Directly after having degassed the VOTTDPz for 5 hours at 250 °C, a deposition for 15 minutes onto Au(111) was carried out. The sample was transfered directly to the STM, and investigated. An image obtained directly after deposition can be seen in Figure 3.4.

Here it can be seen that the image is distorted possibly due to thermal drift, which was a general tendency when imaging directly after a deposition. Therefore the sample was placed and left overnight in the STM hereafter in order to minimize the thermal drift. Submonolayer coverage was realised after 15 minutes of deposition. Larger areas of molecules can be seen, growing from the stepedges of the Au(111). These larger areas seem to have a structural order of the molecules - lying in rows. Smaller areas with no visible order are also seen growing from the stepedges. No smaller islands of molecules in the middle of the terraces were visible when imaging directly after the deposition.

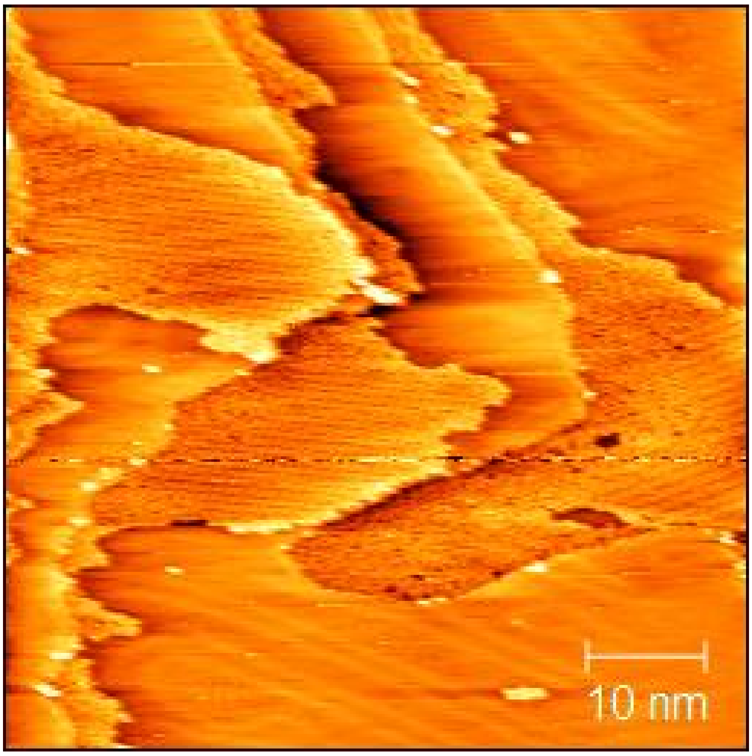

Figure 3.4: Submonolayer coverage of VOTTDPz on Au(111).Areas of VOTTDPz-molecules arranged in ordered larger structures and smaller areas of no visible order at the stepedges. 625Åx625Å, I=0.31nA, V_{bias}=0.5V.

In order to see if the distortion on the images directly after deposition was due to thermal drift, the sample was left in the STM overnight, and investigated the following morning. In Figure 3.5.

Here an approximately 300Åx300Å area of ordered VOTTDPz molecules can be seen in Figure3.5a as well as smaller areas of no visible order growing from the other stepedges. The ordered area has grown between two stepedges on the Au(111) surface and what appears to be ordered diagonal rows of molecules are visible. In Figure 3.5b which is a zoom in on the area in (a), the rows of molecules become more pronounced, but some areas around the stepedge as well as at the outline of the area goes from ordered to disorganised - broken some places by small "holes". This could be indicative of the molecules having grown from the right side terrace, to the left, since the order starts on the left side, and breaks at the right side. Figure 3.5c shows yet another zoom in on the same area displayed in (a) and (b). Here individual features become more visible. It appears that each row in the ordered structure is made up of triangular units having 3 small spherical subunits in each. VOTTDPz has a clover like structure, which cannot be seen on this image although it is possible, that the molecules are not lying completely flat on the

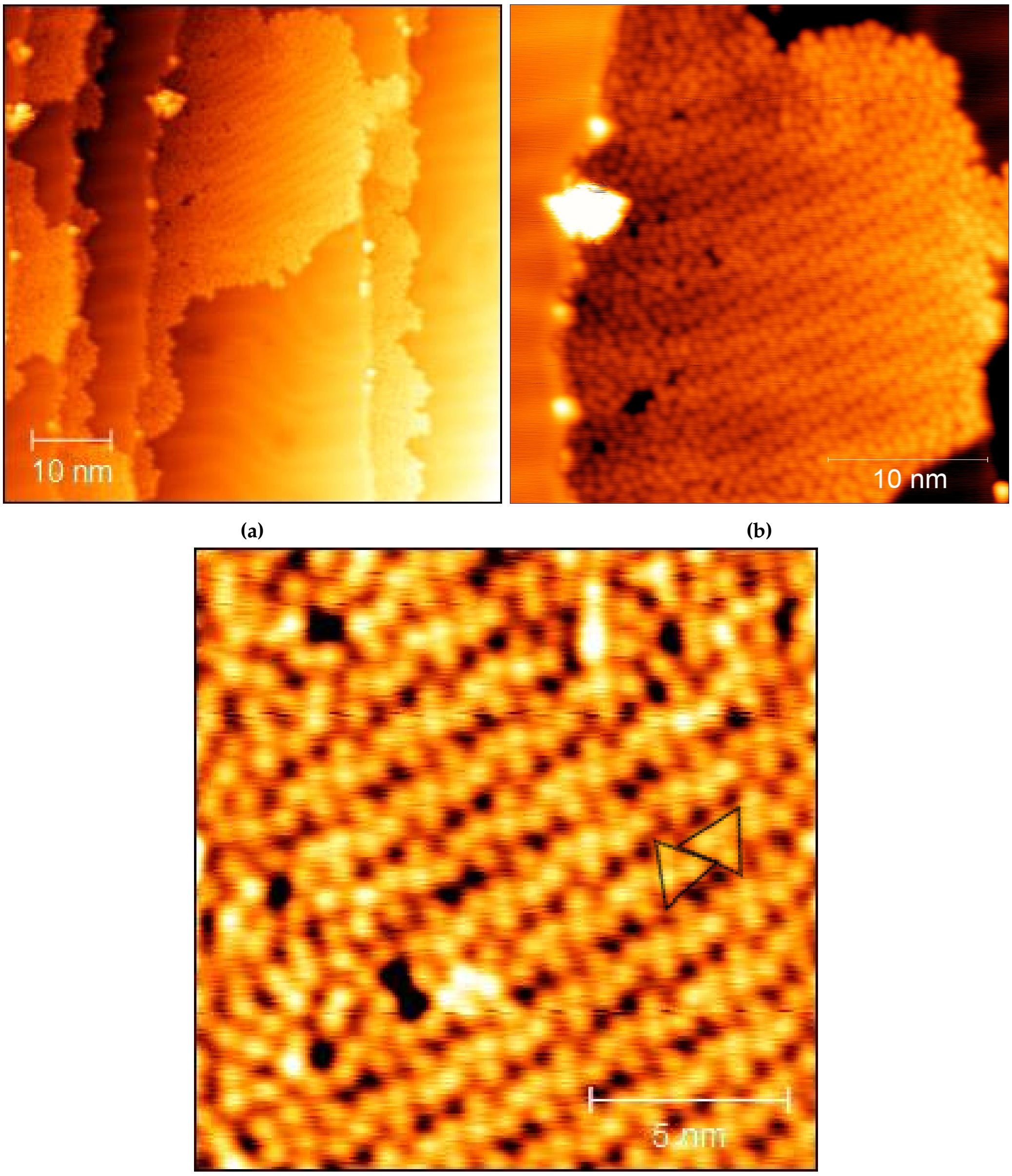

(a) (b)

(c)

Figure 3.5: Images obtained of VOTTDPz molecules on Au(111) from the first deposition after having let the sample stay in the STM overnight. (a) 625Åx625Å image of approximately 300Åx300Å area of ordered VOTTDPz molecules. (b) 312Åx312Å image taken of area shown in (a). (c) 156Åx156Å image taken of area shown in (a) and (b). Triangular insets shows the building block for the rows and appears to have smaller "subunits" in each building block. I=0.31 nA, V_{bias}=0.8V for all pictures.

surface, but are somehow overlapping, hiding one of the "leafs" of the molecules, though this has not been supported by literature, but is a speculation.

3.2.2 Investigation of Bias and Tunnel Current Dependency

A large area of ordered molecules was found, which can be seen in Figure 3.6.

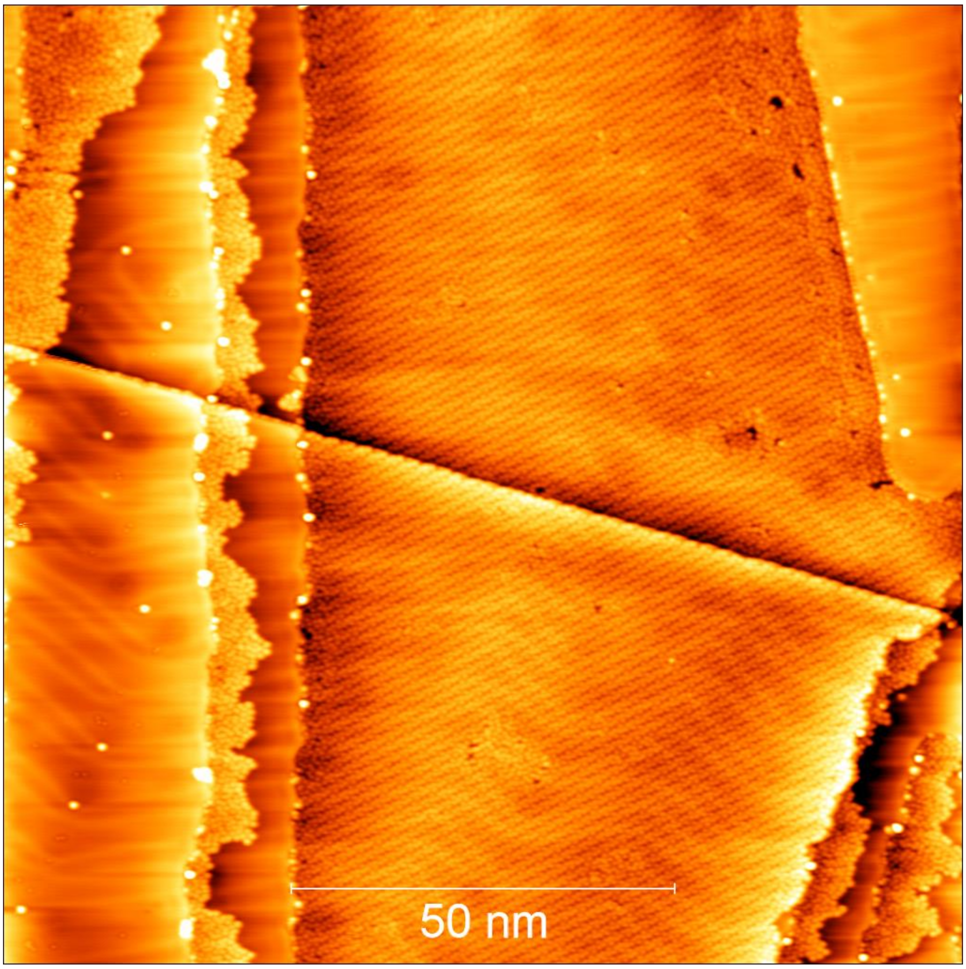

Figure 3.6: 125nm x 125nm image of ordered area of VOTTDPz. The area of order is suspended between two stepedges. Visible through the molecules is the herringbone structure of Au(111). Smaller areas of molecules are seen growing from the other stepedges, with no visible order. Bright spots appear in the elbows of the herringbone structure of Au(111), as well as on the stepedge. I=0.31nA, V_{bias}=0.5V

This area is the largest ordered area found on Au(111), and is the closest to monolayer coverage that has been achieved in this study. The area of order extends between two stepedges, covering a whole terrace. The order is only broken few places throughout the area. From the other stepedges seen in the image smaller areas of molecules are seen having no visible order. Noteworthy is that all of these areas are not sterically compressed between two stepedges. Bright spots appear in the elbows of the herringbone structure of Au(111) as well as on the stepedges.

Though as these individual spots were to large to be a single molecule, and upon further investigation did not have the distinct molecule-like features, the spots were speculated to be impurities.
The ordered area of molecules appear to have their order starting from the left, and is broken at the right side stepedge, indicative of a growth-site on the left. The herringbone structure of Au(111) is visible through the layer of ordered molecules, which could indicate that the surface of Au(111) is not altered by the molecules.

An investigation of the Bias dependency on the appearance of the molecules were carried out on this ordered area. A difference between positive and negative bias applied, can be seen in Figure 3.7.

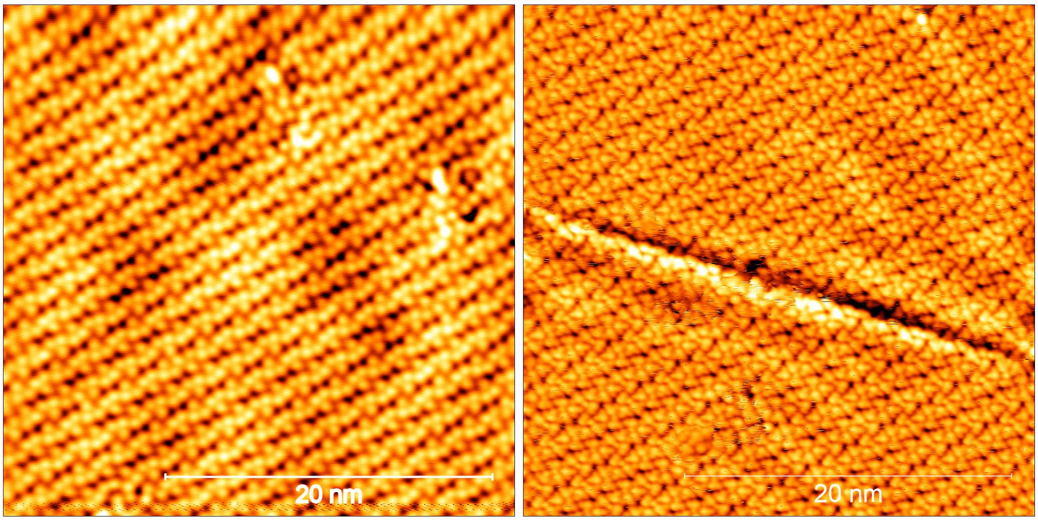

(a) (b)

Figure 3.7: Area of ordered VOTTDPz molecules on Au(111), I=0.31 nA and the area is 312Å x 312Å for both pictures. (a) Taken at positive bias of 0.5 V. Small triangular units with spherical subunits are seen. (b) Taken at negative bias of -0.8 V. Small triangular units with very sharp corners are seen.

On Figure 3.7a the triangular building blocks with 3 spherical units are seen throughout the ordered area of molecules at a positive bias of 0.5 V. This changed significantly when applying a negative bias of -0.8 V to the ordered area as can be seen in Figure 3.7b. Here many small triangular subunits are seen, and no spherical features are visible anymore. These subunits are even harder to combine to what should be a single VOTTDPz molecule. What is also interesting is the lack of small bright spots, that should be more visible at negative bias voltages as found by Hou et al. and can be seen in Figure 1.9(b).

The bias dependency was further investigated in the range from -2 V to 2 V in steps of 100 mV, but the appearance of the molecules did not vary from the ones shown in Figure 3.7. Though later a great example of the dependence of the state of the tip on the appearance of the molecules was found, and can be seen in Figure 3.8.

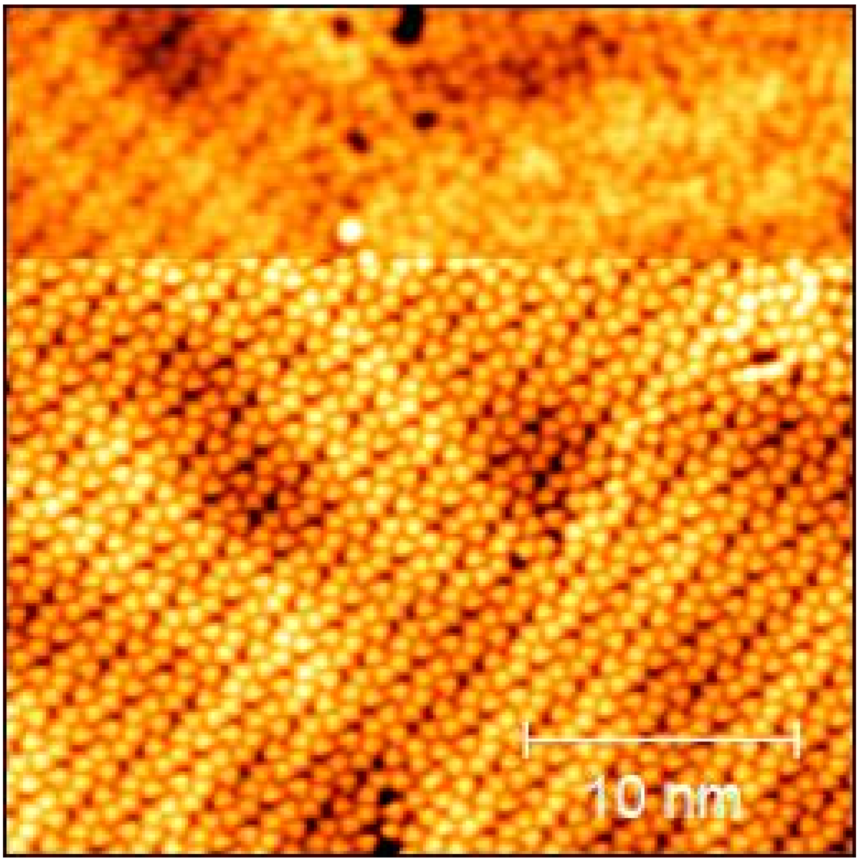

Figure 3.8: Area of ordered VOTTDPz molecules on Au(111). Here it is seen how the state of the needle changes during a scan resulting in the more spherical and "blurry" shapes, turning into welldefined sharper triangular shapes. 312Å x 312Å area, I= 0.21 nA, V_{bias}=0.8 V.

Here the spherical subunits, which appears a bit blurry, becomes well defined triangular shapes when the state of the needle changes. This phenomena of the needle changing states was a reoccuring thing through many of the measurements of this study. And when the needle changed state, the same triangular subunits as seen in Figure 3.8 would appear.

To investigate the apparent height of the molecules a height profile was extracted setting the bare Au(111) surface as zero and dragging a line over the outer molecules of an ordered area. This is visualized in Figure 3.9.
As can be seen in Figure 3.9b, the heightdifference between a terrace and one of the small subunits is approximately 0.18 nm. Furthermore it can be seen that the

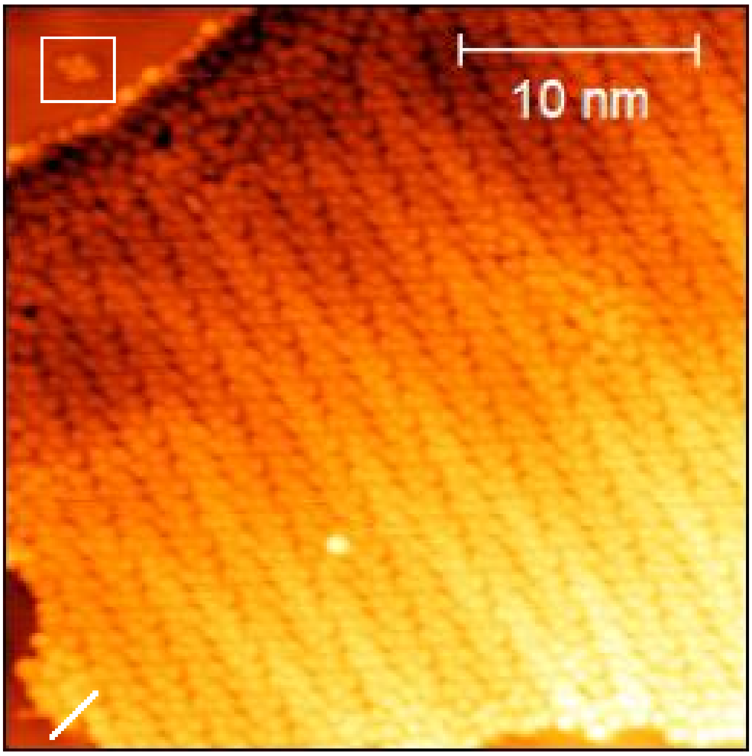

(a)

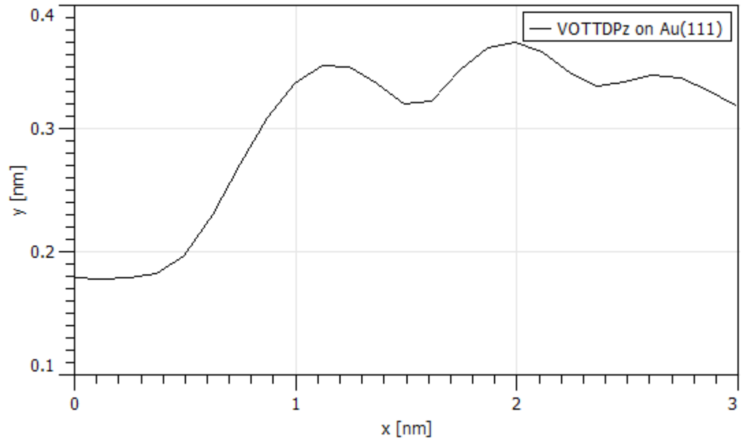

(b)

Figure 3.9: (a) 312Å x 312 Å overview of ordered area of VOTTDPz molecules on Au(111). White line in the bottom left corner shows the line from which the height profile in (b) is drawn. The white bordered inset in the upper left corner shows what appears to be a VOTTDPz-molecule consisting of 4 small spherical subunits. I= 0.18 nA, V_{bias} = -0.8 V. (b) shows the height profile in nm extracted from (a).

height do not vary significantly from center to center of two neighboring subunits.

The study performed by Miyoshi et al. found the bond length between the V and O to be 1.609 Å, and that the vanadylgroup was not in plane with the ligand, but 0.566 Å above it. Thought it is important to remember that these finding were of the crystal structure, and not of the molecules on a surface. Therefore the apparent height of 0.18 nm could indicate the molecules being flatlying on the Au(111) surface in this project.
On Figure 3.9a a white-bordered inset is visible in the top left corner. This inset surrounds what appears to be a single VOTTDPz-molecule, and was therefore investigated as can be seen in Figure 3.10.

In Figure 3.10a arrows denoting the axis of the VOTTDPz-molecule are drawn. It can be seen that the horizontal arrow is longer than the vertical axis, which should not be the case since VOTTDPz is a symmetrical molecule. Though Hou et al. found the same behaviour, as can be seen in Figure 1.9(c). When looking at the extrapolated height profile in Figure 3.10b the dotted line denotes the line drawn through the shorter molecular axis, whereas the solid line denotes the line drawn through the longer molecular axis. Here it can be seen that the maximum height of the entity is 0.15 nm, though this is uncertain, since it can also be seen from the two graphs, that they do not have the same "zero", meaning the terrace appeaers to vary a bit in apparent height. Furthermore the entity appears to be lower compared to the subunits measured in Figure 3.9b. The entity appears to be a bit larger than the individual molecules found by Hou et al. seen in Figure 1.9(b) and (c). This could be explained by the STM not being calibrated properly, although the great agreement between interatomic distance found on Au(111) in this project and in the literature - as mentioned in Chapter2 - works against this reason.

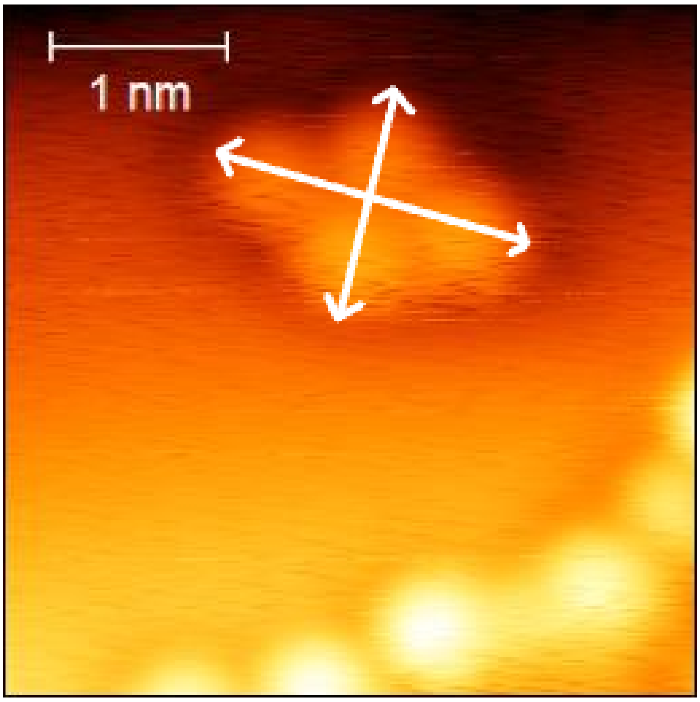

(a)

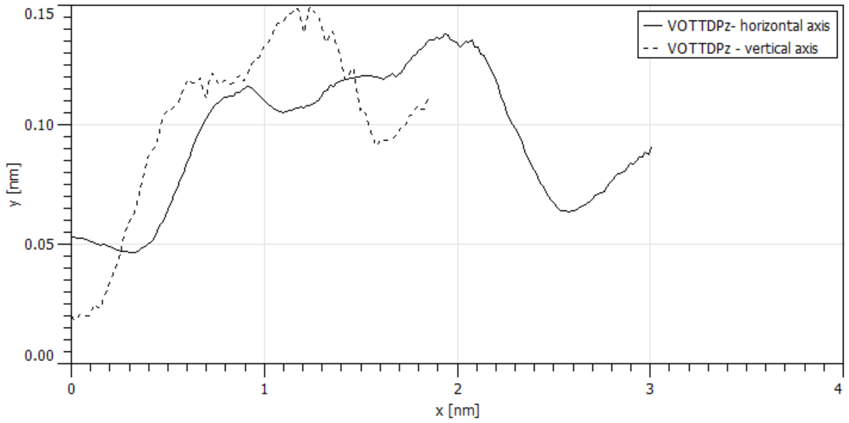

(b)

Figure 3.10: (a) 40Å x 40Å image of what appears to be a single VOTTDPz molecule. 4 spherical subunits in close proximity, in a clover like shape. A horizontal (long arrow) and vertical axis (short arrow) denotes the molecule axes, and furthermore acts the two lines from which a height profile of the molecule was drawn. I= 0.18 nA, V_{bias}= -0.8 V. (b) Height profile plotted from the two arrows seen in (a). Here the solid line denotes the horizontal axis of the molecule, whereas the dotted line denotes the vertical axis of the molecule. The heights are given in nm.

3.2.3 Annealing at Low Temperatures of VOTTDPz/Au(111) System

In order to see if the deposited VOTTDPz molecules would structurally arrange themselves differently if supplied with energy, annealing at low temperatures (being 54 °C on the thermocouple on the heating stage) was carried out. The effect of the annealing can be seen in Figure 3.11.

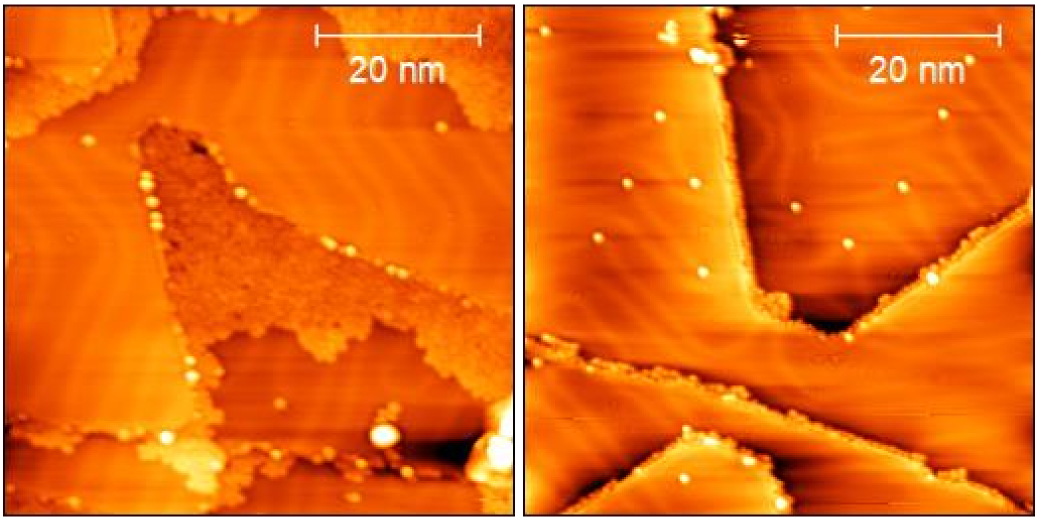

(a) **(b)**

Figure 3.11: 625Å x 625Å overviews of the VOTTDPz/Au(111) system. (a) Shows the system before annealing. Relatively large areas of disorganised molecules can be seen growing from the stepedges. I= 0.3 nA, V_{bias} = -0.8 V. (b) Shows the system after annealing to a temperature of 54 °C on the thermocouple. Here very few molecules are seen, though a mixture of single entities are seen on the terraces as well as on the stepedges. I=0.3 nA, V_{bias}= 0.5 V.

After annealing almost no larger aggregates or ordered structures of molecules were found on the Au(111) surface. The difference in coverage is visualised in Figure 3.11. The disappearance of molecules after annealing at such a low temperature is indicative of the molecule-substrate interaction being very low, even though the sulfur-atoms (though only 4 in VOTTDPz) normally have a high affinity towards gold. Since no studies utilizing annealing of VOPc has been found, a comparison between the thermal stability of VOTTDPz and VOPc cannot be made, although the VOTTDPz should in theory bind more strongly to the substrate. Since almost no molecules were present after the first annealing, no further annealing at higher temperatures were carried out in this project.

3.3 VOTTDPz deposited on Ag(111)

Deposition of VOTTDPz on Ag(111) was carried out at 250-270 °C for 15-25 minutes.

Scanning on several areas of the Ag(111) sample, mainly areas of disorganized VOTTDPz-molecules were found, as can be seen in Figure 3.12.

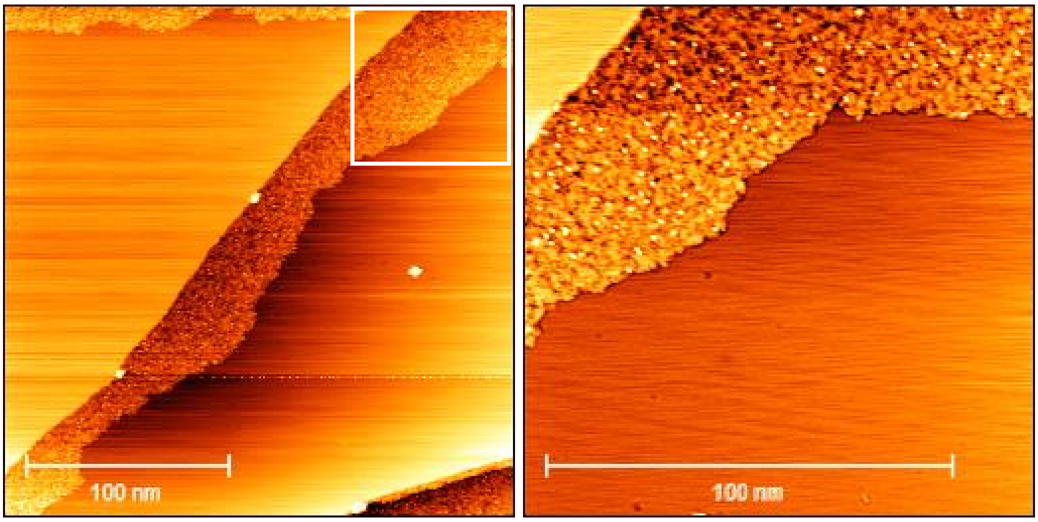

(a) (b)

Figure 3.12: (a) 2500Å x 2500Å overview of VOTTDPz molecules on Ag(111). Relatively large terraces are present. Molecules arrange themselves in aggregates near the stepedges. Inset with white border indicates where image (b) was taken. (b) A 1250Å x 1250Å zoom in of the marked area in (a). Here the disorganisation of the molecules become more apparent. No single molecules or islands of molecules are visible on the terraces. I=0.2 nA, V_{bias}= 0.5 V for both pictures.

The general tendency when scanning the Ag(111) surface after a deposition is visualised in Figure 3.12. No single molecules or small islands of molecules were seen on the terraces during any scan of the Ag(111) surface. VOTTDPz molecules mainly is present near stepedges in aggregates. Visible in the areas of molecules are several very bright spots, which could be either the vanadylgroups or a VOTTDPz-molecule on top of another. A height profile was made in order to figure this out. The line and area of which this was extrapolated from can be seen in Figure 3.13.

Here it can be seen that a line is drawn from the Ag(111) terrace (the zero point), and through both the small spherical units, as well as a bright dot. The height profile is shown in Figure 3.13b. The small spherical unit has an apparent height of approximately 0.15 nm in agreement with the height of an entity found on Au(111), and the bright dot has a height of approximately 0.25 nm. Furthermore the width of the bright dot is approximately 1 nm in correspondence with the size of a VOTTDPz molecule as previously mentioned. Though the apparent height of the bright spot is more than that of a single spherical unit and of the height of the suspected single VOTTDPz molecule found on Au(111), but is more in agreement with the height of a single molecule as stated by Miyoshi et al. and could be due to the molecule not being "bound" to the surface, but stacked on top of another.

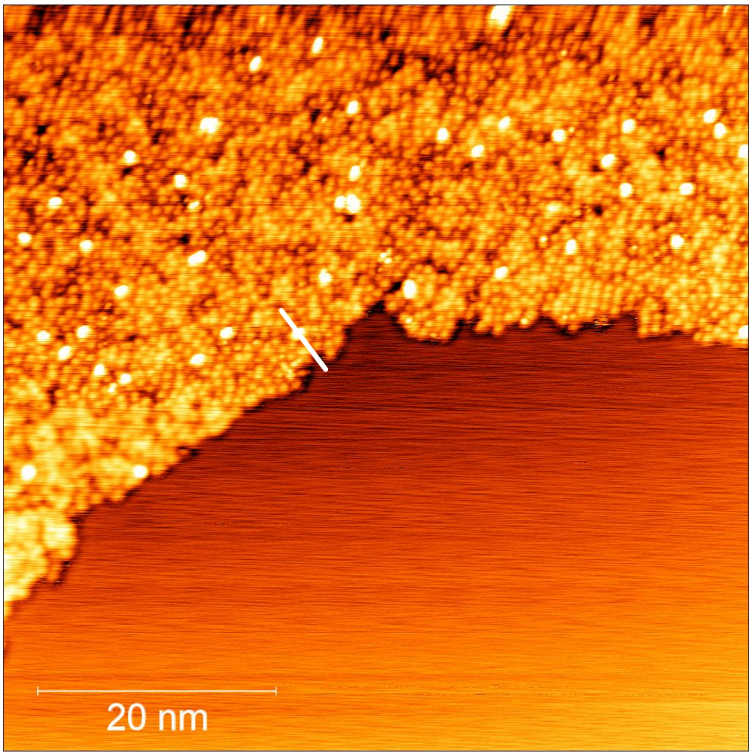

(a)

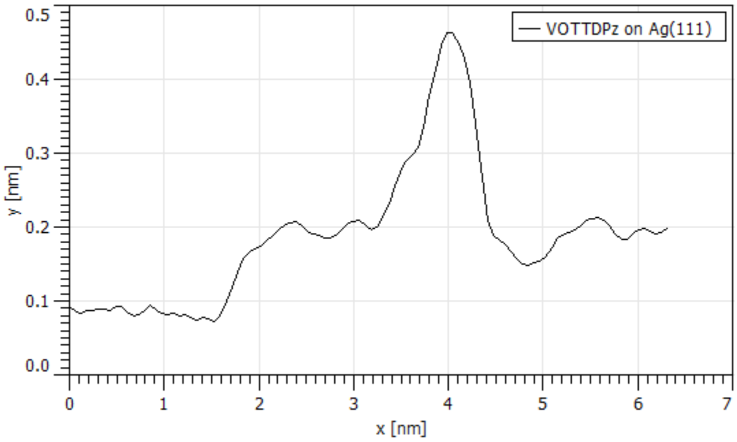

(b)

Figure 3.13: 625Å x 625Å zoom in of Figure 3.12b. The white line is denoting the line used to extrapolate the height profile shown in (b) and is running through both the small spherical units as well as a bright dot. I = 0.22 nA, V_{bias}= 0.5 V. (b) Height profile extrapolated from the white line drawn in (a). Height and distance is measured in nm.

Ordered areas of VOTTDPz molecules were also found on Ag(111), though not as frequently as on Au(111). In general these ordered areas on Ag(111) was larger than those on Au(111), and one such area is shown in Figure 3.14.

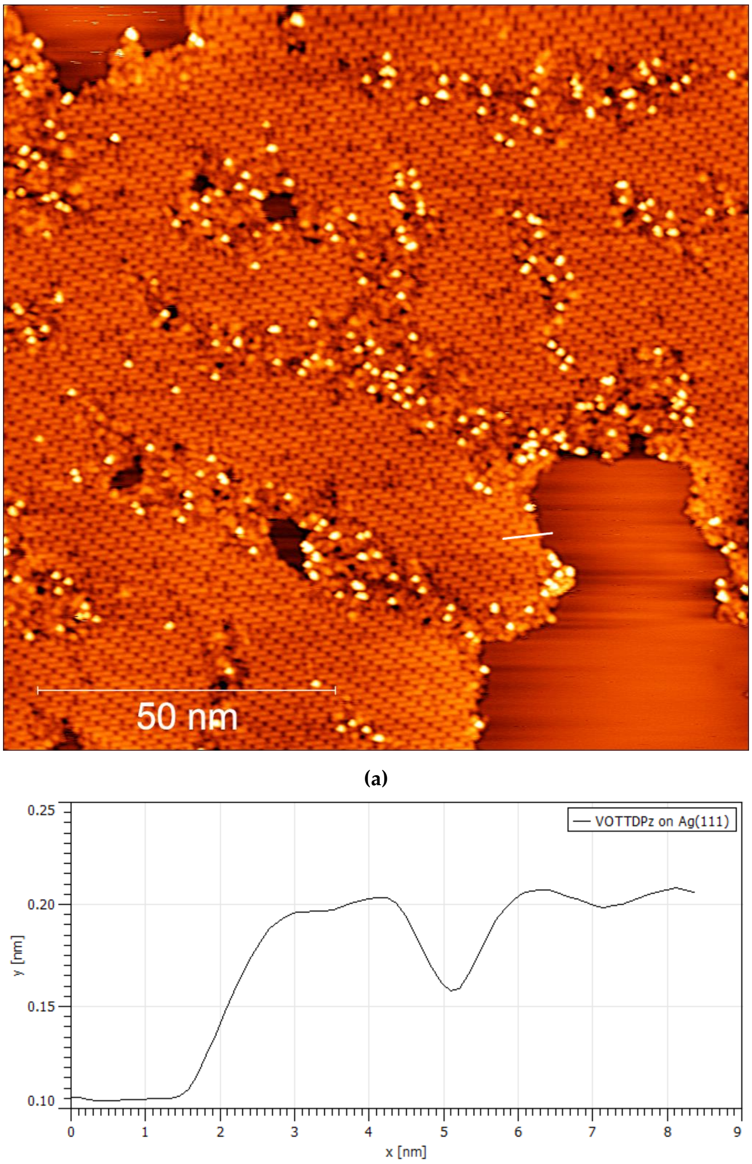

(a)

(b)

Figure 3.14: 1250Å x 1250Å zoom in on a larger ordered area of molecules found on Ag(111). "Brick"-like building blocks can be seen which together forms the ordered structure. Bright dots appear scattered randomly throughout the structure and larger areas of disorganization is present. A white line drawn denotes the extrapolation-points of the height profile shown in (b). I=0.082 nA, V_{bias}= 0.5 V. (b) shows the extrapolated height profile of two of the "bricks". The zero point is set at the Ag(111) surface.

Areas like the one seen in Figure 3.14 was usually of 150nm x 150 nm in size or bigger, which was the general tendency for ordered areas found on Ag(111). The ordered structure appears as a "brick-wall", consisting of smaller rectangular building blocks which is significantly difference than the appearance of VOTTDPz in ordered structures on Au(111). Furthermore the ordered structures would grow from a stepedge, but did not have to be confined sterically by another stepedge on the other side. The average terrace-size on Ag(111) was also significantly larger than on Au(111) in this study. In the ordered area several smaller areas of disorganization can be seen, as well as many bright spots residing in these disorganized areas. In Figure 3.14b the extrapolated apparent height of two "bricks" is seen. The apparent height from a terrace and to the center of a "brick" is approximately 0.10 nm, which is smaller than that of the spherical units on both Ag(111) and Au(111).

A zoom in of the ordered are presented above can be seen in Figure 3.15

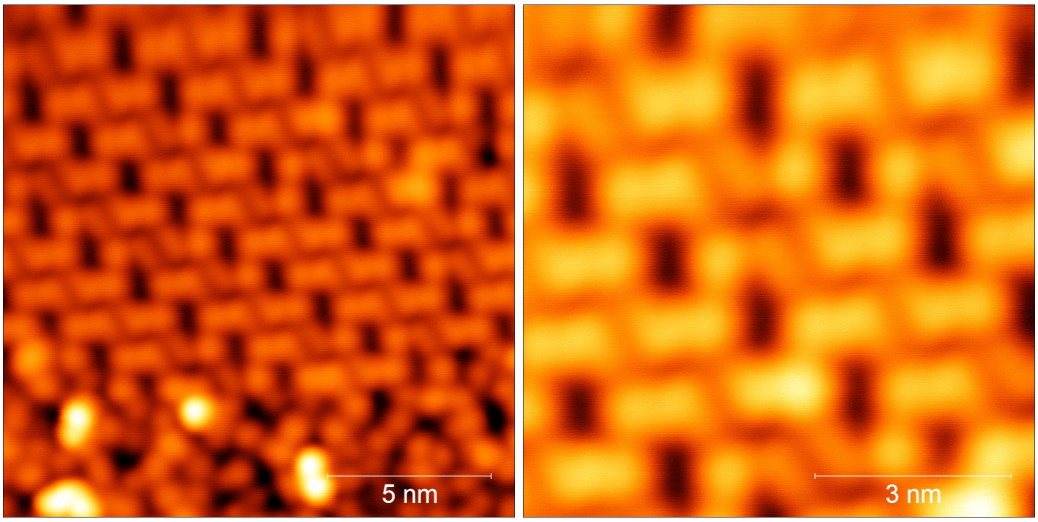

(a) **(b)**

Figure 3.15: (a) 156Å x 156Å zoom in of the area in Figure 3.14a. Here the "brick"-like building blocks is more pronounced. Visible bright spots and spherical units are also visible, breaking the order. (b) 68Å x 68Å zoom in of (a). Each building block appears to consist of two spherical units in very close proximity. Holes in the "brick-wall" can be seen. I=0.082 nA, V_{bias} = 0.5 V for both pictures.

Here the "brick"-like building blocks are more pronounced and gaps/holes in the ordered structures can be seen after every second building block in a line. Furthermore it appears as if every "brick" is consisting of two spherical units. The dimensions of the "bricks" is approximately 1.3 nm x 0.8 nm. The clover like structure of VOTTDPz is not visible at all indicating the molecules in something else than a flatlying configuration on the substrate.

The bias dependency on the appearance of the VOTTDPz molecules was also carried out on the same ordered area. At negative bias-voltages the appearance did not change significantly, until a very low negative bias (-25 mV) was applied. A comparison between a higher negative bias and the lower negative bias can be seen in Figure 3.16.

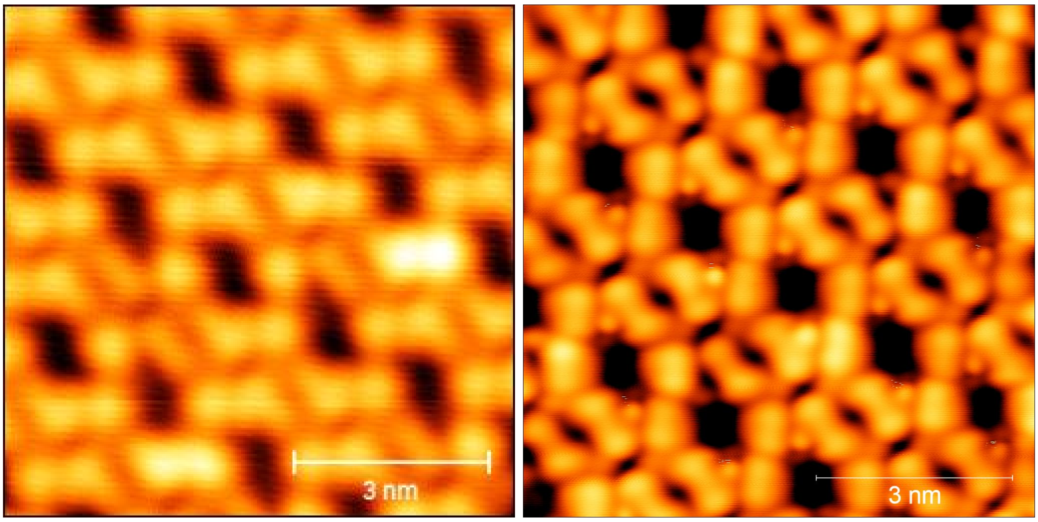

(a) (b)

Figure 3.16: 68Å x 68Å image of the same area as in Figure 3.15 but with applied negative bias. (a) Applied bias was -0.8 V. No significant change in appearance from positive bias can be seen. (b) Applied bias was -25 mV. Here a drastic change in appearance is seen in comparison to (a). Clear features can be seen - larger "peanut"-shaped entities, with small spheres protruding. I=0.3 nA for both pictures.

Here it can be seen that the small applied bias leads to much more resolved features of the ordered structure. "Peanut"-shaped entities with small protruding spheres can be seen. It has been speculated if one "peanut" with a sphere is the VOTTDPz molecule standing up on the substrate. Though the previously measured height profiles with an apparent height of 0.10 nm is in disagreement with this idea, since the apparent height should be around 1 nm, if the molecule was standing on its side. The length of the "peanut" is in good agreement with the size of a single VOTTDpz molecules, although the width of the peanut in addition with the attached sphere is approximately 0.7-0.8 nm, which is almost 4 times the height of a single VOTTDPz molecule.

3.3.1 Annealing at Low Temperatures on the VOTTDPz/Ag(111) System

Annealing the VOTTDPz/Ag(111) system was done at 54 and 74 °C measured on the thermocouple of the heating stage. After heating to 54 °C with no visible change in structure or loss of molecules, the sample was heated to 74 °C.

The result of this can be seen in Figure 3.17

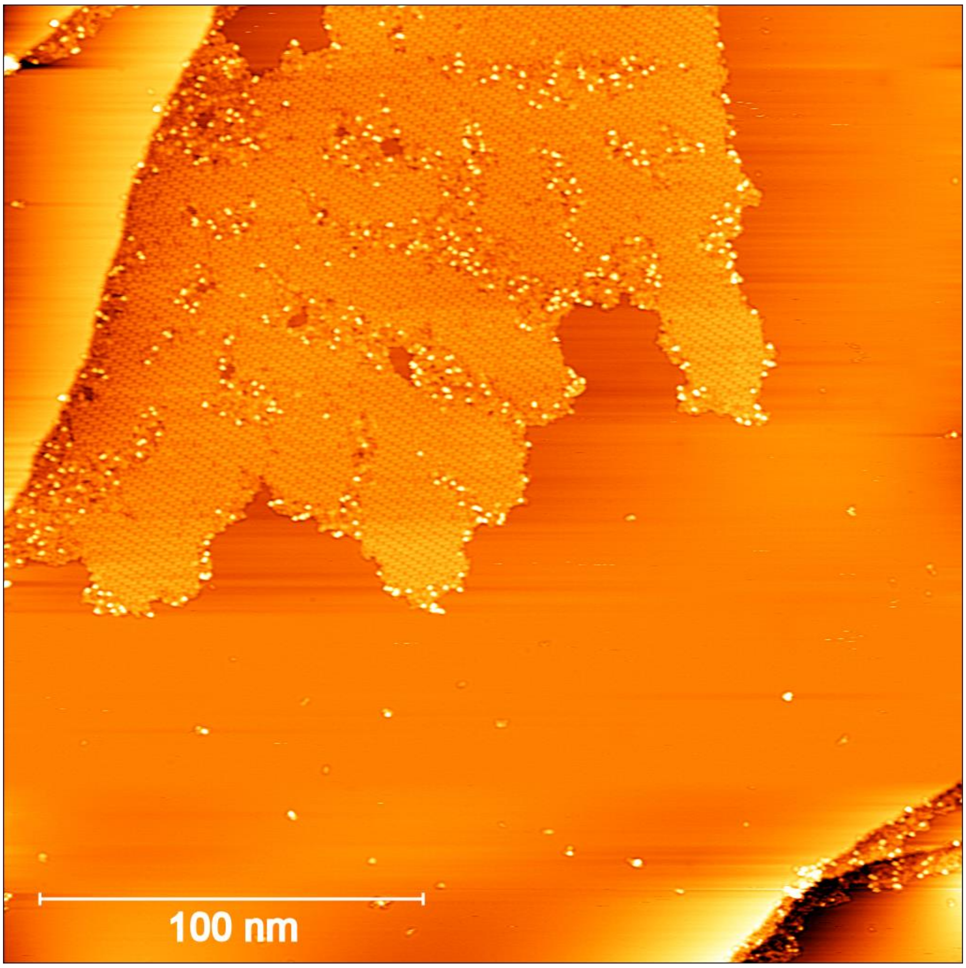

Figure 3.17: 2500Å x 2500Å overview of the Ag(111) surface and molecule-coverage after annealing to 74 °C. Molecules in aggregates are visible from the stepedges, as well as a very large ordered area of molecules. I=0.082 nA, V_{bias}=0.5 V.

Here a very large ordered structure can be seen growing from a stepedge and far out onto a terrace. Smaller areas of disorganised molecules around the outlying stepedges are visible. There seems to be no significant loss of molecules after annealing the system to 74 °C, which is indicative of the VOTTDPz/Ag(111) system being thermally more stable than the VOTTDPz/Au(111) system. This could be due to the less noble nature of Ag(111) compared to Au(111), binding the molecules more strongly to the surface. An investigation of annealing at higher temperatures was not carried out in this study.

Chapter 4

Conclusion, Summary and Outlook

The scope of this project was to replicate the study performed by Hou et al. of depositing VOTTDPz onto Au(111) in order to compare the observed structures in comparison to VOTTDPz deposited on Ag(111). A direct replication was not realised, since the observed ordered structures of VOTTDPz on Au(111) differed significantly in this study compared to that of Hou et al. Individually resolved VOTTDPz molecules were not obtained in this project. The main difference between these two experiments were the temperature at which the images were taken. In this project a temperature of 77K was present during image acquisition, whereas a temperature of 4.7K was utilized in the study of Hou et al. The temperature could help to see the features of individual molecules more easily. But since the ordered structures appeared so different in this project, the temperature alone can not be the sole reason for the difference. In order to further replicate this study, coverage dependency should be investigated, since monolayer coverage was not realised in this project. It was not possible in this project to distinguish the O-up or O-down configuration of the VOTTDPz-molecules. Height profiles extrapolated on the ordered structure of Au(111) could be indicative of an arrangement of flat-lying VOTTDPz-molecules, whereas the height-profiles extrapolated from the ordered structures of Ag(111) led to more questions than answers. Here the speculation of the molecules standing on the side was debunked by the very low height of the entities. In both the case of VOTTPDz on Au(111) and Ag(111) it was not possible to measure intermolecular distances of the molecules as well as the orientation hereof in the ordered structures, since the individual molecules was not resolved. On Ag(111) bright spots that could have been indicative of the vanadyl-group, was speculated to be a VOTTDPz-molecule on top of another due to the extrapolated height profiles. The height of a bright spot was around 2.5 nm, and the height of a single molecule as found by Miyoushi et al. was approximately 2.1 nm. This could be indicative of a difference in apparent height depending on how close the molecule is to the substrate.

Here the molecule on top of another would be screened from the surface, and therefore not bound as tightly. In order to resolve the individual molecules, the kinetics of the deposition could be investigated for future work. Here a "frozen-in" state could possibly lead to molecules trapped on the terraces individually, making them easier to resolve. Another proposal could be to utilize a more reactive substrate (for example Cu(111)), in order to bind the molecules more tightly to the substrate - this could also lead to an investigation of whether this more reactive substrate would make the system more stable thermally. Finally the electronic and magnetic properties could be investigated by means of STS in order to see if these properties is altered significantly by means of the substrate onto which the molecules are deposited, and if they change depending on whether the VOTTDPz molecules are in a disorganised or organised state.

Bibliography

[1] George M. Whitesides, John P. Mathias, and Christopher T. Seto. Molecular self-assembly and nanochemistry: A chemical strategy for the synthesis of nanostructures. *Science*, 254(5036):1312–1319, 1991.

[2] Angelika Kühnle. Self-assembly of organic molecules at metal surfaces. *Current Opinion in Colloid and Interface Science*, 14(2):157–168, 2009.

[3] Simone Ghidinelli, Sergio Abbate, Giuseppe Mazzeo, Lorenzo Paoloni, Elisa Viola, Claudio Ercolani, Maria Pia Donzello, and Giovanna Longhi. Characterization of tetrakis(thiadiazole)porphyrazine metal complexes by magnetic circular dichroism and magnetic circularly polarized luminescence. *Chirality*, 32(6):808–816, 6 2020.

[4] Olesia Snezhkova, Felix Bischoff, Yuanqin He, Alissa Wiengarten, Shilpi Chaudhary, Niclas Johansson, Karina Schulte, Jan Knudsen, Johannes V Barth, Knud Seufert, Willi Auwärter, and Joachim Schnadt. Iron phthalocyanine on Cu(111): Coverage-dependent assembly and symmetry breaking, temperature-induced homocoupling, and modification of the adsorbate-surface interaction by annealing. *J. Chem. Phys*, 144:94702, 2016.

[5] Tianchao Niu, Jialin Zhang, and Wei Chen. Molecular Ordering and Dipole Alignment of Vanadyl Phthalocyanine Monolayer on Metals: The E ff ects of Interfacial Interactions. (111), 2014.

[6] Cornelius Krull. *Electronic structure of metal phthalocyanines on Ag (100)*. Number 100. 2012.

[7] P A Stuzhin, E M Bauer, and C Ercolani. Tetrakis(thiadiazole)porphyrazines. 1. Syntheses and Properties of Tetrakis(thiadiazole)porphyrazine and Its Magnesium and Copper Derivatives. Technical report, 1998.

[8] Yasuhito Miyoshi, Kouji Takahashi, Takuya Fujimoto, Hirofumi Yoshikawa, Michio M. Matsushita, Yukio Ouchi, Mikael Kepenekian, Vincent Robert, Maria Pia Donzello, Claudio Ercolani, and Kunio Awaga. Crystal structure, spin polarization, solid-state electrochemistry, and high

n-type carrier mobility of a paramagnetic semiconductor: Vanadyl tetrakis(thiadiazole)porphyrazine. *Inorganic Chemistry*, 51(1):456–462, 2012.

[9] Jie Hou, Yu Wang, Keitaro Eguchi, Chihiro Nanjo, Tsuyoshi Takaoka, Yasuyuki Sainoo, Kunio Awaga, and Tadahiro Komeda. Inter-molecule interaction for magnetic property of vanadyl tetrakis(thiadiazole) porphyrazine film on Au(111). *Applied Surface Science*, 440:16–19, 2018.

[10] Dodecon Nanotechnology GmbH.

[11] S. B. Darling, A. W. Rosenbaum, Yi Wang, and S. J. Sibener. Coexistence of the (23 3) Au(111) reconstruction and a striped phase self-assembled monolayer. *Langmuir*, 18(20):7462–7468, 2002.

[12] C. Julian. Chen. *Introduction to scanning tunneling microscopy.* Monographs on the Physics and Chemistry of Materials. Oxford University Press, Oxford, 2nd ed. edition.

[13] Scanning tunneling microscopy.

[14] R Nathans and A Paoletti. PHYSICAL REVIEW LETTERS (unpublished). TUNNELLING FROM A MANY-PARTICLE POINT OF VIEW. Technical Report 2, 1959.

[15] Thomas S. Smith, Russell LoBrutto, and Vincent L. Pecoraro. Paramagnetic spectroscopy of vanadyl complexes and its applications to biological systems. *Coordination Chemistry Reviews*, 228(1):1–18, 2002.